CP3-17-23
LPT-Orsay-17-35
DESY 17-124

September 5, 2017

Neutrino masses, leptogenesis and dark matter from small lepton number violation?

Asmaa Abada[a], Giorgio Arcadi[b], Valerie Domcke[c,d] and Michele Lucente[e]

[a] *Laboratoire de Physique Théorique, CNRS, Univ. Paris-Sud, Université Paris-Saclay, 91405 Orsay, France*
[b] *Max Planck Institut für Kernphysik, Saupfercheckweg 1, 69117 Heidelberg, Germany*
[c] *AstroParticule et Cosmologie (APC)/Paris Centre for Cosmological Physics (PCCP), Université Paris Diderot, Paris, France*
[d] *Deutsches Elektronensynchrotron (DESY), Notkestrasse 85, 22765 Hamburg, Germany*
[e] *Centre for Cosmology, Particle Physics and Phenomenology (CP3) Université catholique de Louvain, Chemin du Cyclotron 2, 1348 Louvain-la-Neuve, Belgium*

arXiv:1709.00415v1 [hep-ph] 1 Sep 2017

Abstract

We consider the possibility of simultaneously addressing the baryon asymmetry of the Universe, the dark matter problem and the neutrino mass generation in minimal extensions of the Standard Model via sterile fermions with (small) total lepton number violation. Within the framework of Inverse and Linear Seesaw models, the small lepton number violating parameters set the mass scale of the active neutrinos, the efficiency of leptogenesis through a small mass splitting between pairs of sterile fermions as well as the mass scale of a sterile neutrino dark matter candidate. We provide an improved parametrization of these seesaw models taking into account existing experimental constraints and derive a linearized system of Boltzmann equations to describe the leptogenesis process, which allows for an efficient investigation of the parameter space. This in particular enables us to perform a systematic study of the strong washout regime of leptogenesis. Our study reveals that one can have a successful leptogenesis at the temperature of the electroweak scale through oscillations between two sterile states with a natural origin of the (necessary) strong degeneracy in their mass spectrum. The minimal model however requires a non-standard cosmological history to account for the relic dark matter. Finally, we discuss the prospect for neutrinoless double beta decay and for testing, in future experiments, the values of mass and different active-sterile mixings required for successful leptogenesis.

Contents

1 Introduction **1**

2 Lepton number violation in minimal low-scale frameworks **3**

2.1 Constraints 4

2.2 Minimal particle content: the LSS-ISS model 5

2.3 Minimal realizations of the Inverse Seesaw: ISS(2,2) and ISS(2,3) 7

3 Leptogenesis **9**

3.1 Weak washout regime 13

3.2 Beyond the weak washout regime 14

4 Numerical analysis and results **18**

4.1 The LSS-ISS model 18

4.1.1 Parameter space 18

4.1.2 Leptogenesis in the LSS-ISS 22

4.2 The Inverse Seesaw 24

4.2.1 Parameter space 24

4.2.2 Leptogenesis in the ISS(2,2) 27

4.2.3 Leptogenesis and dark matter in the ISS(2,3) 31

5 Conclusion **34**

A Some useful formulas for simplifying the kinetic equations **36**

A.1 Decay rates 36

A.2 Weak washout limit 38

A.3 Diagonalization of the equation for the sterile sector 40

B The parameter space for DM in the ISS(2,3) **41**

References **42**

1 Introduction

The generation of the baryon asymmetry of the Universe (BAU) is one of the major puzzles of modern particle physics and leptogenesis is among the most popular solutions. One of the simplest realizations of leptogenesis is the so called "thermal leptogenesis" [1] , which relies on the out-of-equilibrium decay of heavy right-handed (RH) neutrinos and in which baryogenesis is in general tied to the seesaw mechanism for the light neutrino mass generation [2–6].

At low seesaw scales, thermal leptogenesis is however very fine-tuned and difficult to implement, and one must consider alternatives to generate any lepton asymmetry. An interesting alternative is the so-called "ARS" mechanism, first proposed by Akhmedov, Rubakov and Smirnov [7], in which a lepton asymmetry is produced by the CP-violating oscillations of a pair of heavy sterile neutrinos. This mechanism was then implemented in the ν-MSM [8–10] with the aim of simultaneously addressing the issues of i) neutrino mass generation, ii) the BAU, and iii) of providing a viable dark matter (DM) candidate. In this approach, three RH neutrinos $N_R^{1,2,3}$ were added to the Standard Model (SM), the lightest of them (with mass at the $\sim$ keV scale) is almost sterile - in the sense that its mixings to the active light neutrinos and to the other sterile fermions are negligible - playing thus the role of the DM candidate. The two other (heavier) RH neutrinos are responsible for the generation of the light neutrino masses and of the lepton asymmetries, both at early times, giving rise to the BAU, and at later times, enabling the production of the correct relic DM abundance [11]. The strong condition in order to achieve all these tasks simultaneously is that the heavier two RH neutrinos are almost degenerate in mass. Variants of this scenario capable of achieving a successful BAU while accommodating neutrino data, in some cases without in addition providing a DM candidate, have also recently been considered in [12–18].

Remarkably, the crucial condition of degeneracy in the heavy spectrum can find a natural origin in scenarios in which the smallness of light neutrino masses is due to a small violation of the total lepton number (LNV) [19]. This can be achieved when, for instance, the Inverse Seesaw mechanism (ISS) [20, 21] is embedded into the SM. Here the light neutrino masses m_ν are proportional a Majorana mass parameter $\mu = \xi\Lambda$, which violates lepton number by two unites ($\Delta L = 2$). The seesaw scale Λ sets the mass scale of the additional heavy SM singlets. In the limit $\xi \to 0$ lepton number conservation is restored and $m_\nu \to 0$ (coining the name 'inverse' seesaw). This is achieved by introducing at least two additional sets of SM singlet fermions (referred to RH neutrinos and sterile fermions) with opposite lepton number assignment. These combine into pseudo-Dirac pairs with masses of $\mathcal{O}(\Lambda)$ and mass differences of $\mathcal{O}(\mu)$, and depending on the realization, may also result in a sterile fermion with a mass scale μ, which can account for the relic DM abundance, see for example, [22–24]. The available neutrino data is accommodated within the ISS for large values of the Yukawa couplings and a comparatively low seesaw scale Λ, which renders this mechanism phenomenologically appealing. A second low-scale seesaw mechanism based on a small LNV is the

Linear Seesaw (LSS) [25,26], which also requires the introduction of two types of fermionic singlets (RH and sterile) with opposite lepton number assignment, and in which the smallness of neutrino masses is also linked to the small $\Delta L = 2$ violation of the total lepton number. The difference with respect to the ISS is that the LNV arises from additional small Yukawa couplings of the 'sterile' fermions to the left-handed (LH) neutrinos. The resulting light neutrino mass scale is linearly dependent on these Yukawa couplings, coining the name for this mechanism.

In a previous study [17] we investigated the generation of the BAU in low energy realizations of the LSS and ISS models. The analysis conducted in [17] was mostly focused on a minimal phenomenological model based on adding two singlet fermions with opposite lepton number to the SM, which are almost degenerate in mass and form a pseudo-Dirac pair. Their mass splitting, as well as the masses of the light neutrinos, are determined by two small parameters, a Majorana mass term and a LNV Yukawa coupling, violating the total lepton number by two units; this scenario essentially resembles an ISS realization extended by a LSS mass term, model we refer to as "LSS-ISS". Ref. [17] included a detailed analysis of leptogenesis in the region of parameter space satisfying the "weak washout" condition, i.e. where the Yukawa couplings are sufficiently weak to strongly suppress any erasing of the generated asymmetry. In the "strong washout" regime, the lack of an efficient method to calculate the baryon asymmetry restricted the analysis to a proof of existence of viable solutions. While successfully accounting for the observed baryon asymmetry, the solutions in the weak washout regime predicted active-sterile mixing angles which are too small to be detectable in current and upcoming experiments. The analysis of [17] further included the ISS(2,2) model, the most minimal realization of the ISS, which requires the addition of two RH neutrinos and two steriles to the SM, leading to two pseudo-Dirac pairs in the heavy sector, as shown in [22]. In this case we found that existing neutrino data forces the mass splitting within the two pseudo-Dirac pairs to be too large to achieve successful leptogenesis in the weak washout regime.

The present work aims at refining the analysis and extending the results presented in [17]; the distinctive new aspects of the present study are summarized below. We have derived a systematic perturbative expansion of the set of coupled Boltzmann equations (BE) describing the generation of the lepton asymmetry, which is particularly suited to efficiently describe the strong and intermediate washout regime.[1] Moreover, in addition to the production and decay of heavy neutrinos through top quark radiation considered in [17], we include the production via gauge boson radiation through the exchange of a lepton doublet in the t-channel. In the limit of vanishing leptonic chemical potentials the rate of these gauge-mediated processes was found to exceed the one associated to the top quark by about a factor of three [28, 29]. To include these processes in the current study,

[1] We point out the complementary method presented in Ref. [27], which provides an analytical solution deep in the strong washout regime.

we re-derive the kinetic equations including all scattering processes considered in [28, 29], which we re-evaluate in the presence of small leptonic chemical potentials. We thus complete our previous derivation [17] and correct the source term for sterile neutrinos by taking into account thermal effects of gauge boson interactions in the set of coupled BE, estimating their impact in generating the BAU (see also [18, 27] for similar studies); we further take into account the effect of "spectator processes". Throughout this paper, we have consistently used the Fermi-Dirac statistic rather than the Maxwell-Boltzmann one used in [17]. Our improved treatment allows, for the scenarios considered in [17], a full coverage of the parameter space corresponding to the "strong washout" regime, where we find that not only the LSS-ISS model provides successful leptogenesis, but also the ISS(2,2). Moreover, we find that the strong washout regime allows for solutions with sufficiently high active-sterile mixings to be experimentally observable in the near future. Furthermore, we extend our study to the ISS(2,3) model, where in addition to two pseudo-Dirac pairs (already present in the ISS(2,2) model), a lighter mostly sterile state is present in the mass spectrum, which under suitable conditions can play the role of the DM component. We investigate whether viable leptogenesis could be simultaneously compatible with the existence of this stable state and with a solution to the DM problem.

Finally, in these extensions of the SM with extra neutrinos (RH or steriles), the effective mass in neutrinoless double beta decay ($0\nu\beta\beta$) is modified and incorporates the additional CP-violating phases and the extra mixing angles. It has been shown in [30–32] that if sterile neutrinos are present, a signal in $0\nu\beta\beta$ does not necessarily imply an inverted hierarchy (IH) for the light neutrino spectrum. Part of this project is devoted to study the impact of the additional neutral fermions considered in our minimal scenarios (LSS-ISS , ISS (2,2) and (2,3)) on the effective mass in $0\nu\beta\beta$ when leptogenesis is at work.

The remainder of this paper is organized as follows. Section 2 introduces the minimal Inverse and Linear Seesaw models as well as the observational constraints on neutrino mas models. The derivation and simplification of the BE responsible for leptogenesis is given in Section 3, additional intermediate results can be found in App. A. Section 4 is dedicated to the results of the numerical parameter scans, including also our approach to parameterizing the above seesaw models in view of existing neutrino data. An analytical approach to understanding these results in the context of the DM problem is given in App. B. We conclude in Section 5.

2 Lepton number violation in minimal low-scale frameworks

Adding new neutrinos to the Standard Model leads to a broad range of new phenomenology. Depending on the mass scale of these neutrinos, they may address open questions in cosmology (leptogenesis, dark matter,..) or lead to interesting signals in laboratory experiments (beam-dump experiments, neutrino-less double beta decay,..). In this study, we focus on minimal low-scale seesaw

frameworks [22] which can account for the observed neutrino masses and mixing with the masses of the neutrinos responsible for generating the BAU not exceeding about 50 GeV. In the following, we will first recall the relevant constraints in this mass range and then turn to the explicit seesaw models. This will lead to the introduction of new fermion fields belonging to two categories: (i) RH neutrinos, which in the interaction basis feature Yukawa interactions with the SM Higgs and lepton doublets and (ii) sterile neutrinos, which have no such couplings. In a slight abuse of notation, we will also apply this categorization to the LSS, in which case the 'sterile' neutrinos in fact have (very suppressed) couplings to the SM. Most of our analysis will be however carried out in the mass basis, where the new states are in general a mixture of the RH and sterile (and active) components. We will thus more generally refer to states dominated by RH and/or sterile components as (SM) singlets. In all minimal scenarios considered here, the lightest active neutrino will be massless.

2.1 Constraints

Beside complying with neutrino oscillation data [33,34], the extension of the SM by singlet fermions (RH or sterile ones) is subject to important constraints, which strongly constrain their masses as well as the active-sterile mixing. We will briefly summarize in this subsection the constraints adopted throughout all our analysis.

Perturbative unitarity [35–40] requires $\frac{\Gamma_{\nu_i}}{m_{\nu_i}} < \frac{1}{2}\,(i = 1, N)$.[2] Additional bounds arise from electroweak precision tests [41–44] and non-standard interactions [45–47]. Sterile fermions can also induce potentially large contributions to charged lepton flavor violating (cLFV) observables, such as charged lepton flavor violation at low energy like in $\mu - e$ conversion in nuclei, radiative and three-body decays ($\mu \to e\gamma$, $\mu \to eee$) [48–56], as well as cLFV at high energy in Higgs [57–62] and neutral Z boson decays [63–66]; sterile fermions can also impact leptonic and semi-leptonic meson decays [44,67–70]. They may further contribute to lepton flavor conserving but CP-violating observables (due to the additional CP violating phases) such as the charged lepton electric dipole moments [71–73]. We moreover take into account negative results from searches for monochromatic lines in the spectrum of muons from $\pi^\pm \to \mu^\pm \nu$ decays [69, 74] as well as those from searches at the LHC [60–62]. It is worth stressing that particularly severe constraints arise from the violation of lepton universality in leptonic meson decays [44, 67, 68, 70]. In the near future, neutral fermions with masses in the GeV range can be searched in experiments such as NA62 [75], SHiP [76, 77], FCC-ee [78] and LBNF/DUNE [79].

[2] Noticing that the leading contribution to Γ_{ν_i} is due to the charged current term, the perturbative unitarity condition translates into the following bounds:

$$m_{\nu_i}^2\, \mathbf{C}_{ii} < 2\, \frac{M_W^2}{\alpha_w} \qquad (i \geq 4)\,, \tag{1}$$

where $\alpha_w = g_w^2/4\pi$, and $\mathbf{C}_{ii} = \sum_{\alpha=1}^{3} \mathcal{U}_{\alpha i}^* \mathcal{U}_{\alpha i}$, $\mathcal{U}$ being the lepton mixing matrix.

The presence of source(s) of LNV in the considered frameworks may also induce consequences on the effective mass in the amplitude of the neutrinoless double beta decay rate [80], which is defined, in the case where the SM is extended by N sterile fermions as [81]:

$$m_{0\nu\beta\beta} \simeq \sum_{i=1}^{N} \mathcal{U}_{ei}^2 \, p^2 \frac{m_i}{p^2 - m_i^2} \ , \tag{2}$$

where $p^2 \simeq -(125 \text{ MeV})^2$ is the virtual momentum (an average estimate over different decaying nuclei) of the propagating neutrino. Notice that the additional mixings and possible new CP-violating Majorana phases might enhance the effective mass, potentially rendering it within experimental reach, or even leading to the exclusion of certain regimes due to conflict with the current bounds - the most recent results on neutrinoless double beta decay have been obtained by the EXO-200 experiment [82] and by KAMLAND-Zen [83].

The final constraint is of cosmological origin. The neutrinos involved in the low-energy seesaw cannot be too light, otherwise their lifetimes would be of the same order as the timescale of Big Bang Nucleosynthesis (BBN). Their decays into SM states at this time would have severe consequences on the synthesis of the light nuclei. To avoid this possibility, we will assume a conservative lower bound of 100 MeV [84] on the masses of the new states and impose that their life times do not exceed 1 second.[3]

2.2 Minimal particle content: the LSS-ISS model

The type-I seesaw mechanism provides a simple explanation for the light neutrino masses: Introducing RH neutrinos with a Majorana mass M_N and which share a Dirac mass m_D with the active neutrinos, the diagonalization of the mass matrix yields the light neutrino masses $m_\nu = m_D M_N^{-1} m_D$ which are inversely proportional to the heavy Majorana mass scale. The introduction of additional sterile fermions changes this picture, and depending on the underlying GUT breaking mechanism and the model parameters, different seesaw contributions to m_ν may be dominant, allowing for small active neutrino masses m_ν despite lowering the mass scale of the additional SM singlet fermions. In this section we introduce the LSS-ISS model, which is a phenomenological low-scale seesaw model with minimal particle content, based on the introduction of the two small LNV parameters found in the Linear [25, 26] and Inverse [20, 21] Seesaw models.

The SM spectrum is extended by two RH neutrinos N_R^1, N_R^2 at the mass scale Λ with opposite lepton number, more specifically $+1$ for N_R^1 and -1 for N_R^2. In the interaction basis the new states are coupled to the active sector via Yukawa couplings Y_α and $\epsilon Y'_\alpha$, respectively. With $|Y'| \sim |Y|$ and $\epsilon \ll 1$, the latter couplings violates lepton number by a small amount. The second LNV parameter is introduced as a Majorana mass $\mu = \xi\Lambda$ for the sterile neutrinos. The assignment ϵ, ξ

[3] Except for the potential DM candidate in the ISS(2,3), whose life time exceeds the age of the Universe.

1 is technically natural, since lepton number is restored in the limit of $\epsilon, \xi \to 0$. The neutrino global mass term of Lagrangian reads

$$-\mathcal{L}_{m_\nu} = n_L^T \; C \; \mathcal{M} \; n_L + \text{h.c.}, \tag{3}$$

where

$$n_L \equiv \left(\nu_L^e, \nu_L^\mu, \nu_L^\tau, N_R^{1\,c}, N_R^{2\,c}\right)^T , \quad \text{and} \quad C = i\gamma^2\gamma^0 \; , \tag{4}$$

and with the full mass matrix of the neutrino sector

$$\mathcal{M}^{(\nu)} = \; \Lambda \begin{pmatrix} 0 & 0 & 0 & \frac{1}{\sqrt{2}} Y_1 v/\Lambda & \frac{1}{\sqrt{2}} \epsilon Y_1' v/\Lambda \\ 0 & 0 & 0 & \frac{1}{\sqrt{2}} Y_2 v/\Lambda & \frac{1}{\sqrt{2}} \epsilon Y_2' v/\Lambda \\ 0 & 0 & 0 & \frac{1}{\sqrt{2}} Y_3 v/\Lambda & \frac{1}{\sqrt{2}} \epsilon Y_3' v/\Lambda \\ \frac{1}{\sqrt{2}} Y_1 v/\Lambda & \frac{1}{\sqrt{2}} Y_2 v/\Lambda & \frac{1}{\sqrt{2}} Y_3 v/\Lambda & 0 & 1 \\ \frac{1}{\sqrt{2}} \epsilon Y_1' v/\Lambda & \frac{1}{\sqrt{2}} \epsilon Y_2' v/\Lambda & \frac{1}{\sqrt{2}} \epsilon Y_3' v/\Lambda & 1 & \xi \end{pmatrix} , \tag{5}$$

where v is the Higgs boson vacuum expectation value.

To illustrate the structure of Eq. (5), let us consider a toy model with a single generation for the active neutrinos. In this case the mass matrix has the following form,

$$\mathcal{M}^{(\nu)} = \begin{pmatrix} 0 & Yv/\sqrt{2} & \epsilon Y' v/\sqrt{2} \\ Yv/\sqrt{2} & 0 & \Lambda \\ \epsilon Y' v/\sqrt{2} & \Lambda & \xi\Lambda \end{pmatrix} , \tag{6}$$

which can be decomposed as

$$\mathcal{M}^{(\nu)} = \mathcal{M}_0 + \Delta\mathcal{M}_{ISS} + \Delta\mathcal{M}_{LSS} \; . \tag{7}$$

The lepton number conserving mass matrix $\mathcal{M}_0$ is given by

$$\mathcal{M}_0 = \begin{pmatrix} 0 & \frac{1}{\sqrt{2}} Yv & 0 \\ \frac{1}{\sqrt{2}} Yv & 0 & \Lambda \\ 0 & \Lambda & 0 \end{pmatrix} , \tag{8}$$

and its diagonalization gives rise to the mass spectrum

$$m_\nu = 0 \, , \quad M_{1,2} = \sqrt{|\Lambda|^2 + \frac{1}{2}|Yv|^2} \; . \tag{9}$$

The perturbation of the latter matrix by two sources of lepton number violation encoded in $\Delta\mathcal{M}_{ISS}$ (proportional to the LNV parameter ξ) and $\Delta\mathcal{M}_{LSS}$ (proportional to the LNV parameter ϵ) leads to the matrix of Eq. (6). Considering only the perturbation $\Delta\mathcal{M}_{ISS}$ leads to the Inverse Seesaw pattern [20, 21] while considering the second perturbation, $\Delta\mathcal{M}_{LSS}$, leads to a Linear Seesaw pattern [26].[4] Allowing both $\xi \neq 0$ and $\epsilon \neq 0$ leads to a mixed Linear and Inverse Seesaw mechanism, a model we refer to as "LSS-ISS". Compared to Eq. (9), the mass scale m_ν of the lightest neutrino and the mass splitting $\Delta m^2_{\rm PD}$ between the two heavy neutrinos are now non-zero,

$$m_\nu \simeq 2\epsilon \frac{m_D^2}{\Lambda}\,, \qquad \Delta m^2_{\rm PD} = M_2^2 - M_1^2 = 2\xi\Lambda^2\,, \tag{10}$$

where $m_D = Yv/\sqrt{2} \simeq Y'v/\sqrt{2}$. This structure immediately generalizes to the full mass matrix of Eq. (5): the mass scale of the active neutrinos is set by the LNV parameter ϵ, whereas the second LNV parameter ξ controls the small mass splitting within the heavy pseudo-Dirac pair - a crucial parameter for ARS leptogenesis. Further details of this model, including the perturbative diagonalization of the full matrix (5), can be found in Ref. [17]. This neutrino mass model can account for the observed neutrino oscillation data, a suitable parametrization of the remaining free parameters will be introduced in Sec. 4.1.1.

2.3 Minimal realizations of the Inverse Seesaw: ISS(2,2) and ISS(2,3)

Next we turn to the pure Inverse Seesaw mass generation mechanism [20, 21]. Compared to the previous subsection, this implies $\epsilon = 0$ and we will moreover allow for an independent number of RH and sterile neutrinos ($\#\nu_R \neq 0$ and $\#s \neq 0$). In the case of $\#s = 0$, one recovers the usual type I seesaw realization, which could account for neutrino masses and mixings provided that the number of right-handed neutrinos is at least $\#\nu_R = 2$.

The neutrino mass term has the same structure as in Eq. (3), with

$$n_L \equiv \left(\nu_L^e,\, \nu_L^\mu,\, \nu_L^\tau,\, \nu_{R,i}{}^c, s_j\right)^T\,, \tag{11}$$

where $\nu^c_{R,i}$ ($i = 1, ..\#\nu_R$) and s_j ($j = 1, ..\#s$) are RH neutrino fields and additional fermionic gauge singlets, respectively. The neutrino mass matrix in Eq. (3) has the form,

$$\mathcal{M} \equiv \begin{pmatrix} 0 & d & 0 \\ d^T & 0 & n \\ 0 & n^T & \xi\Lambda \end{pmatrix}\,, \tag{12}$$

[4] A non-vanishing value of the $(2,2)$ entry of the matrix Eq. (6), $\mathcal{M}^{(\nu)}_{22} = \xi'\Lambda$, would correspond to an additional LNV violation by two units, which does not generate neutrino masses at tree level but does it only at loop level [30,85]. These loop corrections will be relevant only if $\xi' \gtrsim 1$, meaning for regimes of a large lepton number violation. However, as in our approach to leptogenesis we focus on models with an approximate lepton number conservation, we will not pursue this option any further here.

where $d, n, \xi\Lambda$ are complex mass matrices. The Dirac mass matrix d arises from the Yukawa couplings to the SM Higgs boson, $\widetilde{H} = i\sigma^2 H$,

$$d_{\alpha i} = \frac{v}{\sqrt{2}} Y^*_{\alpha i}, \qquad \mathcal{L} \ni Y_{\alpha i} \overline{\ell^\alpha_L} \widetilde{H} \nu^i_R + \text{h.c.}, \quad \ell^\alpha_L = \begin{pmatrix} \nu^\alpha_L \\ e^\alpha_L \end{pmatrix}, \tag{13}$$

while the matrix $\xi\Lambda$, instead, contains the Majorana mass terms for the sterile fermions s_j. This is the only LNV parameter in the ISS models. The sub-matrix n is $\#\nu_R \times \#s$ matrix with entries of order Λ. By assigning a opposite leptonic charge to ν^c_R and s, one ensures that the off-diagonal terms are lepton number conserving, while $s^T C s$ violates the lepton number by two units. The feature of the ISS is that the entries of the matrix ξ can be made small in order to accommodate for $\mathcal{O}$(eV) masses of (mostly) active neutrinos, while having large Yukawa couplings. This is not in conflict with naturalness since the lepton number is restored in the limit of $\xi \to 0$ and all along this work we impose the above matrices to fulfill a *naturalness criterion*, $|\xi\Lambda| \ll |d| < |n|$ [22].

Concerning the singlet fermions, ν_R and s, since there is no direct evidence for their existence (and because they do not contribute to anomalies), their number is unknown. In [22] it was shown that it is possible to construct several distinct realizations of the ISS, reproducing the correct neutrino mass spectrum while complying with the constraints listed above, thereby strongly preferring a normal ordered active neutrino spectrum. More specifically, it was shown that, depending on the number of additional fields, the neutrino mass spectrum obtained for each ISS realization is characterized by either 2 or 3 mass scales, corresponding to the light neutrino mass scale m_ν, the mass scale of the heavy pseudo-Dirac pair(s) $m_{\rm PD}$ and, only if $\#s > \#\nu_R$, an intermediate scale $m_{\rm DM}$:

$$m_\nu \simeq \xi\Lambda \frac{d^2}{n^2} = \frac{\xi (Yv)^2}{2 m_{\rm PD}}, \quad m_{\rm PD} \simeq n \simeq \Lambda, \quad m_{\rm DM} \simeq \xi\Lambda. \tag{14}$$

The mass splitting within the pseudo-Dirac pair(s) is given by

$$\Delta m^2_{\rm PD} \simeq 2\,\xi\, m^2_{\rm PD}. \tag{15}$$

This allows to identify two truly minimal ISS realizations [22], the ISS (2,2) model, which corresponds to the SM extended by two RH neutrinos and two additional sterile fermions, and the ISS (2,3) model, where the SM is extended by two RH neutrinos and three sterile states. In agreement with the discussion above, the physical mass spectrum of both models presents two pairs of pseudo-Dirac neutrinos. The ISS(2,3) features, in addition, an intermediate mass scale mostly sterile neutrino. As extensively discussed in [22, 23], this additional state can have mass both in the eV range, possibly accommodating a 3+1-mixing scheme at low energies which can be used to interpret the short baseline (reactor/accelerator) anomalies [86], or in the keV range. In this case the mostly sterile neutrino could be a DM candidate providing interesting phenomenology related

to structure formation [87–94] and to indirect detection [95–97]. Related to this last point, it is worth mentioning the hint (not confirmed) of the detection of an X-ray line at approximately the energy of 3.5 keV [98, 99]. In view of more recent analyses both the hints related to reactor anomalies and to the X-ray line appear increasingly disfavored. The reference to them is only intended to highlight the rich phenomenology of the scenario under study. A suitable parameterization of the ISS models, taking into account observational constraints, will be introduced in Sec. 4.2.1. We finally remark that in the ISS(2,3) the mass of the intermediate sterile state, relevant in our work mostly for DM phenomenology, is tightly related to the mass splitting of the pseudo-Dirac pairs. As will be discussed more extensively in the following this is a key parameter for the achievement of a viable BAU.

3 Leptogenesis

The neutrino mass models of the previous section feature one (or several) pair(s) of pseudo-Dirac neutrinos, whose mass splitting(s) is (are) governed by a small LNV parameter, and whose overall mass scale can be set to the GeV - TeV range. These are the crucial ingredients to implement leptogenesis through neutrino oscillations [7]: Starting from a negligible abundance of these heavy neutrinos in the early Universe, a pseudo-Dirac pair is thermally produced just before the electroweak (EW) phase transition. Due to the small mass splitting, rapid oscillations of the neutrinos within the pseudo-Dirac pair occur, entailing a CP-violating background for the active neutrinos. The active neutrinos hence experience an effective CP-violating potential, similar to the MSW effect of matter [100]. This induces a lepton asymmetry in the active species, which in turn back-reacts to the pseudo-Dirac pairs, further enhancing the CP asymmetry of this sector. This way a lepton asymmetry is generated both in the sector of the SM states and in the sector of the new SM singlet fermions. For simplicity we will label, here and in the next sections, these two sectors as active and singlet sectors, respectively. Note that the leptogenesis process occurs in the highly relativistic regime for the new neutrinos. Their Majorana mass terms are negligible and we can extend the usual definition of lepton number to their different helicity states. For the same reason, the total asymmetry summed over both the active and singlet sectors must vanish. The asymmetries produced in the active and singlet sector are hence of equal value, but have opposite sign. However, sphaleron processes act only on the asymmetry in the SM sector, (partially) converting it into the baryon asymmetry we observe today. In this way, leptogenesis occurs even if the total lepton number is (approximately) conserved. In this section, we first summarize the key equations describing these processes following a series of earlier studies [8–10, 13, 14, 16–18, 27, 101] which have lead to an improved understanding of many aspects in recent years. Some technical details are relegated to Appendix A. In Section 3.1 we summarize the results of our earlier work [17] on the weak washout regime, before developing a new method of solving the differential equations in the

full parameter space of interest, including the strong washout regime, in Section 3.2.

The processes sketched above can be described in the density matrix formalism by two differential matrix equations, one for the singlet neutrinos N and one for the active species L [84],

$$\frac{d\rho_N}{dt} = -i\,[H_N, \rho_N] - \frac{1}{2}\left\{\Gamma^d_N, \rho_N\right\} + \frac{1}{2}\left\{\Gamma^p_N, I - \rho_N\right\}\,, \tag{16}$$

$$\frac{d\rho_L}{dt} = -i\,[H_L, \rho_L] - \frac{1}{2}\left\{\Gamma^d_L, \rho_L\right\} + \frac{1}{2}\left\{\Gamma^p_L, I - \rho_L\right\}\,. \tag{17}$$

Here $\rho_{N,L}$ denote the density matrices of the singlet and active species, $\Gamma^{p,d}_{N,L}$ are the respective production and decay rates and $H_{N,L}$ are the corresponding Hamiltonians, containing a vacuum part $H^0_{N,L}$ describing the propagation and oscillations, as well as, an effective potential $V_{N,L}$. All quantities are functions of the wave numbers $k_{N,L}$, the temperature T (or equivalently the cosmic time t) and the chemical potential μ_L of the active flavors (arising in a CP-violating background). The equations for the corresponding anti-particles are obtained by substituting: $L \leftrightarrow \bar{L}$, $N \leftrightarrow \bar{N}$, $F \leftrightarrow F^*$ and $\mu_L \leftrightarrow -\mu_L$. Here $F_{\alpha I}$, contained in the production and decay rates, denotes the Yukawa coupling of the singlet neutrinos in their mass eigenbasis,

$$F_{\alpha I} = Y_{\alpha i}\,\mathcal{U}_{iI}\,, \tag{18}$$

with $\mathcal{U}$ denoting the unitary matrix which diagonalizes $(\mathcal{M}^{(\nu)})^\dagger\mathcal{M}^{(\nu)}$. Here α and i run over the active and SM singlet neutrino flavors, respectively, while I runs over the heavy mass eigenstates. Due to the unitarity of the matrix $\mathcal{U}$, $\sum_{\alpha,I}|F_{\alpha I}|^2 \simeq \sum_{\alpha,i}|Y_{\alpha,i}|^2$.

These equations can be significantly simplified by taking the active species to be in thermal equilibrium with a chemical potential μ_L, $\rho_L(k_L, T, \mu_L) = N_D\, f_F(k_L/T, \mu_L)\, I$, with $f_F(k_L/T, \mu_L) = \left[\exp\left(\frac{k_L}{T} - \mu_L\right)\right]^{-1}$ denoting the Fermi-Dirac distribution function with momentum k_L and chemical potential[5] μ_L, computed at the thermal bath temperature T.

We further note that the system studied here contains two small parameters which may be exploited for a perturbative analysis: the entries of the Yukawa matrix $F_{\alpha I}$ and the chemical potentials μ_{L_α}. The latter are directly related to the generated baryon asymmetry, which is why they are expected to be small for all viable parameter points.

Performing these expansions and after some additional manipulations detailed in Appendix A, the production and destruction rates of the singlet neutrinos can be rewritten, to first order in μ_L, as:

$$\begin{aligned}\Gamma^p_N &= f^0_F(y_N)\gamma^0_N F^\dagger F + \delta\gamma^p_N F^\dagger \mu_L F\,,\\ \Gamma^d_N &= (1 - f^0_F(y_N))\gamma^0_N F^\dagger F + \delta\gamma^d_N F^\dagger \mu_L F\,,\end{aligned} \tag{19}$$

[5]Below we will perform a perturbative expansion with respect to the chemical potential; for this reason it is appropriate to define it as a dimensionless quantity by reabsorbing the temperature factor.

where $y_N = k_N/T$ and where we have defined $f_F^0(y_N) \equiv f_F(y_N, 0)$. Moreover,

$$\gamma_N^0 = \frac{T^3}{64\pi^3 k_N^2}\Sigma(y_N)\,, \tag{20}$$

$$\delta\gamma_N^p = -\frac{T^3}{64\pi^3 k_N^2}\left(f_F^{'}(y_N)\Sigma(y_N) + f_F^0(y_N)\Psi(y_N)\right)\,, \tag{21}$$

$$\delta\gamma_N^d = \frac{T^3}{64\pi^3 k_N^2}\left(f_F^{'}(y_N)\Sigma(y_N) + (1 - f_F^0(y_N))\Psi(y_N)\right)\,, \tag{22}$$

where $\Sigma(y_N)$ and $\Psi(y_N)$ are integrals containing the matrix element of the interaction process, (their formal expression is provided in Appendix A), while $f_F^{'} = \frac{df_F^0(y)}{dy}$.

The corresponding decay and production rates of the active species (describing the exact same processes from the point of view of these particles), can be related to Eqs. (20) - (22) by exchanging the order of integration in the integrated decay rates:

$$\begin{aligned}
&\int \frac{d^3k_L}{(2\pi)^3}\Gamma_L^d(k_L) f_F(k_L/T, \mu_L) \\
&\qquad = \frac{1}{N_D}\int \frac{d^3k_N}{(2\pi)^3} f_F^0(k_N/T)\gamma_N^0 F(I - \rho_N(k_N))F^\dagger + \delta\gamma_N^p \mu_L F(I - \rho_N(k_N))F^\dagger\,, \\
&\int \frac{d^3k_L}{(2\pi)^3}\Gamma_L^p(k_L)(1 - f_F(k_L/T, \mu_L)) \\
&\qquad = \frac{1}{N_D}\int \frac{d^3k_N}{(2\pi)^3}(1 - f_F^0(k_N/T))\gamma_N^0 F\rho_N(k_N)F^\dagger + \delta\gamma_N^d \mu_L F\rho_N(k_N)F^\dagger\,.
\end{aligned} \tag{23}$$

The expressions above show that, in general, one has to solve a system of coupled integro-differential equations. It can be however reduced to a system of ordinary differential equations by assuming that the heavy neutrinos fulfill the weaker condition of kinetic equilibrium, $\rho_N(k_N, T)_{IJ} = R_N(T)_{IJ} f_F(k_N/T, \mu_L = 0)$. $N_D = 2$ is an $SU(2)$ factor. With this we can factor out the momentum-independent variable $R_N(T)$ in the integrals above, and replace the integrated rates with thermally averaged destruction and production rates:

$$\langle\gamma(T)\rangle = \frac{\int d^3p\,\gamma(p,T) f_F^0(p/T)}{\int d^3p\, f_F^0(p/T)}\,. \tag{24}$$

Additionally substituting the lepton number densities by an equation directly for the chemical potential,

$$\int \frac{d^3k_L}{(2\pi)^3}\left[f_F(k_L/T, \mu_L) - f_F(k_L/T, -\mu_L)\right] \approx -2\mu_L \int \frac{d^3k_L}{(2\pi)^3} f^{'}(k_L/T) = \frac{T^3}{6}\mu_L \tag{25}$$

$$\rightarrow \mu_{L\alpha} = \frac{6}{T^3}\int \frac{d^3k_L}{(2\pi)^3}\left(\rho_L - \rho_{\bar{L}}\right)_{\alpha\alpha}\frac{1}{N_D}\,, \tag{26}$$

we obtain to first order in μ_L

$$\frac{dR_N}{dt} = -\,i\,[\langle H\rangle, R_N] - \frac{1}{2}\langle\gamma^{(0)}\rangle\left\{F^\dagger F, R_N - I\right\} - \frac{1}{2}\langle\gamma^{(1b)}\rangle\left\{F^\dagger\mu_L F, R_N\right\} + \langle\gamma^{(1a)}\rangle F^\dagger\mu_L F\,, \quad (27)$$

$$\frac{d\mu_{L\alpha}}{dt} = \frac{9\,\zeta(3)}{2N_D\,\pi^2}\left\{\langle\gamma^{(0)}\rangle\left(FR_NF^\dagger - F^*R_{\bar{N}}F^T\right) - 2\langle\gamma^{(1a)}\rangle\mu_L FF^\dagger + \right.$$
$$\left. + \langle\gamma^{(1b)}\rangle\mu_L\left(FR_NF^\dagger + F^*R_{\bar{N}}F^T\right)\right\}_{\alpha\alpha}\,, \quad (28)$$

with

$$\mu_L = \mathrm{diag}(\mu_{L\alpha})\,, \quad \gamma^{(0)} \equiv \gamma_N^0\,, \qquad f_F^0(k_N/T)\,\gamma^{(1a)} \equiv \delta\gamma_N^p\,, \qquad \gamma^{(1b)} \equiv \delta\gamma_N^p + \delta\gamma_N^d\,. \quad (29)$$

Note that the off-diagonal elements of $\rho_L, \rho_{\bar{L}}$ do not enter Eq. (27), and hence it is sufficient to solve Eq. (28) for the diagonal components only, implying that the commutator in Eq. (17) can be dropped. The leading order decay rate $\gamma^{(0)}$ was recently re-evaluated in Ref. [29], taking into account, not only scattering processes involving the top quark, but also processes involving soft gauge bosons of the thermal plasma. This work was extended to account for a finite chemical potential in Ref. [18], thus determining $\gamma^{(1a),(1b)}$ (there labeled $\gamma^{(1),(2)}$, respectively.). The resulting thermally averaged rates are found to be

$$\langle\gamma^{(i)}\rangle = A_i\left[c_{\mathrm{LPM}}^{(i)} + y_t^2 c_Q^{(i)} + (3g^2 + g'^2)\left(c_V^{(i)} - \ln(3g^2 + g'^2)\right)\right]\,, \quad (30)$$

where g, g' denote the (temperature-dependent) SM $SU(2)$ and $U(1)$ gauge couplings, y_t is the top Yukawa coupling, and

$$A_0 = 2A_{1a} = -4A_{1b} = \frac{\pi T}{2304\,\zeta(3)}\,. \quad (31)$$

The numerical values of $c_{LPM,Q,V}^{(i)}$ are reported in Tab. 1 of Ref. [18]. Both $c_Q^{(i)}$ and $c_V^{(i)}$ are found to be T-independent, the temperature dependence of $c_{LPM}^{(i)}$ is so mild that we will neglect it in the following, using $c_{LPM}^{(i)}(T = 10^4\ \mathrm{GeV})$ as a reference value.

So far, we have focused on interactions between the various active and singlet neutrino species which are mediated by the Yukawa coupling F and which modify μ_α, i.e. the total lepton number of the active sector. However, as pointed out in Refs. [102, 103], a further important role is played by the so-called spectator processes. Before the EW phase transition, sphaleron and SM Yukawa mediated processes distribute the asymmetry among the various species of the thermal bath, thereby conserving $B - L$ but violating $B + L$. A simple way to incorporate these processes is to work directly with the differential equation for $B - L$. The production and decay terms for the lepton doublet on the right-hand side of Eq. (28) (now producing $L = -(B-L)$) are in fact the only terms which change $B - L$. Labeling the chemical potential associated with $B - L$ as μ_Δ, this yields

$$\frac{d\mu_{\Delta\alpha}}{dt} = -\,\frac{9\zeta(3)}{2N_D\,\pi^2}\left\{\langle\gamma^{(0)}\rangle\left(FR_NF^\dagger - F^*R_{\bar{N}}F^T\right) - 2\langle\gamma^{(1a)}\rangle\mu_L FF^\dagger\right.$$
$$\left. + \langle\gamma^{(1b)}\rangle\mu_L\left(FR_NF^\dagger + F^*R_{\bar{N}}F^T\right)\right\}_{\alpha\alpha}\,, \quad (32)$$

with μ_L and μ_Δ related [27, 104] through

$$\mu_{L_\alpha} = A_{\alpha\beta}\mu_{\Delta_\beta}\,, \qquad A = \frac{1}{711}\begin{pmatrix} -221 & 16 & 16 \\ 16 & -221 & 16 \\ 16 & 16 & -221 \end{pmatrix}, \tag{33}$$

for $T \lesssim 10^5$ GeV. The conversion of the $B-L$ asymmetry to the observed baryon asymmetry finally introduces the usual sphaleron conversion factor 28/79.

The above simplifications preserve a crucial consistency feature of the framework: the total asymmetry generated in both the active and singlet sectors vanishes, i.e.

$$\begin{aligned} 0 &= \left(\frac{dn_N}{dt} - \frac{dn_{\bar{N}}}{dt}\right) - \mathrm{Tr}\left[\frac{dn_{\Delta\alpha}}{dt}\right] \\ &= \int \frac{d^3k_N}{(2\pi)^3} f_F^0(k_N)\mathrm{Tr}\left[\left(\frac{dR_N}{dt} - \frac{dR_{\bar{N}}}{dt}\right)_{\alpha\alpha}\right] + 2N_D \int \frac{d^3k_L}{(2\pi)^3} f'(k_L)\mathrm{Tr}\left[\frac{d\mu_{\Delta\alpha}}{dt}\right]. \end{aligned} \tag{34}$$

We can now distinguish two phenomenologically different regimes. The weak washout regime, obtained for $|F_{\alpha I}| \lesssim 10^{-7}$, is characterized by $R_N \ll 1$ and $\mu_L \lll 1$, which allows for a perturbative analytical solution of Eqs. (27) and (28) [17]. For larger values of $|F_{\alpha I}|$, R_N grows from initially small values to $|R_N| \sim 1$, inducing sizable washout effects on the final asymmetry. Consequently, the asymmetry μ_L reaches a peak value at intermediate time-scales before washout-processes reduce the value to the one observed today. We find that μ_L is still small enough to serve as an expansion parameter, however the larger values we find here compared to the weak washout regime require a more careful and rigorous treatment of the expansion.

3.1 Weak washout regime

The weak washout regime was studied in detail in Refs. [9, 10, 17]. Starting from Eqs. (27) and (28), an iterative process allows a fast determination of the final baryon asymmetry: in a first step, Eq. (27) is solved in the limit $\mu_L \to 0, R_N \ll 1$; this is inserted into Eq. (28) (neglecting again the terms proportional to μ_L on the right-hand side); the resulting expression for μ_{L_α} is finally re-inserted into Eq. (27), now evaluated to first order in μ_L. As long as μ_L is sufficiently small, this decoupling of the equations is justified and the resulting asymmetry matches the asymmetry obtained in the full system to good accuracy. Moreover, this procedure allows for an analytical estimate of the final asymmetry (see Appendix A.2):

$$Y_{\Delta B} = \frac{n_{\Delta B}}{s} = \frac{2835}{5056}\frac{1}{\pi^{17/6}\,\Gamma(5/6)}\frac{1}{g_s}\sin^3\phi\,\frac{M_0}{T_{\mathrm{W}}}\frac{M_0^{4/3}}{\left(\Delta m^2_{PD}\right)^{2/3}}\,Tr\left[F^\dagger A_{\alpha\beta}\delta_\beta F\right], \tag{35}$$

where Δm^2_{PD} is the difference between the squared masses of the nearly-degenerate heavy neutrinos, $T_{\mathrm{W}} = 140$ GeV is the temperature of the EW phase transition, g_s counts the degrees of freedom

in the thermal bath at $T = T_{\rm W}$, $M_0 \approx 7 \times 10^{17}\,$GeV, $\sin\phi \sim 0.004$ and $\delta = {\rm diag}(\delta_\alpha)$ is the CP asymmetry in the oscillations defined as:

$$\delta_\alpha = \sum_{i>j} {\rm Im}\left[F_{\alpha i}\left(F^\dagger F\right)_{ij} F^\dagger_{j\alpha}\right] \,. \tag{36}$$

Equation (35) has an analogous functional form as found in [17]. To facilitate the comparison of [17] with the results presented here, we highlight the three most important refinements of the present work: Firstly, we are here working with the full Fermi-Dirac distribution function whereas Ref. [17] uses the Maxwell-Boltzmann distribution, which leads to a different overall factor in Eq. (35). Secondly, we are now taking into account soft scatterings of gauge bosons of the thermal plasma on the production and decay rates, whereas Ref. [17] estimated these rates based on top-quark scattering only. These changes are encoded in the definition of $\sin\phi$, which hence takes a different numerical value here compared to [17]. Thirdly, we take into account the re-distribution of the asymmetry in the active sector through spectator processes. Taking the Maxwell-Boltzmann limit of Eqs. (27) and (28), keeping only the top-quark contribution to the scattering rates and taking $A \to I$ in Eq. (33), one recovers precisely the system of equations used in Ref. [17].

3.2 Beyond the weak washout regime

To solve Eqs. (27) and (28) outside the weak washout regime, we will linearize these equations in the small parameters μ_{L_α} and $(\Delta R_N)_{ij} = (R_N - R_{\bar{N}})_{ij}$, which parametrize the asymmetry in the system.

Zeroth order

Let us first consider the equation for the singlet states, Eq. (27). We will first solve it at zeroth order in μ_α, which will provide some useful insight on how to treat the linearized system:

$$\frac{dR_N^{(0)}}{dt} = -i\left[\langle H\rangle, R_N^{(0)}\right] - \frac{1}{2}\langle\gamma^{(0)}\rangle\left\{F^\dagger F, R_N^{(0)} - I\right\} \,. \tag{37}$$

We can now conduct a series of simplifications. First, we perform a change of variables, namely $t \to x \equiv T_{\rm EW}/T$. Second, we note that

$$\langle V_N\rangle = \frac{N_D T}{16} F^\dagger F \frac{\int dy_N\, y_N f(y_N)}{\int dy_N\, y_N^2 f(y_N)} = \frac{N_D T}{16}\frac{4\pi^2}{3\,\zeta(3)}\frac{1}{24} F^\dagger F = \frac{\langle\gamma^{(0)}\rangle}{2\phi^{(0)}} F^\dagger F \,, \tag{38}$$

with

$$\phi^{(0)} = \frac{3\cdot 48\zeta(3)}{N_D \pi^2 T}\langle\gamma^{(0)}\rangle \tag{39}$$

$$= \frac{1}{16\pi}\left[c_Q^{(0)} h_t^2 + c_{LPM}^{(0)} + (3g^2 + g'^2)\left(c_V^{(0)} + \log\left(\frac{1}{3g^2 + g'^2}\right)\right)\right] \,. \tag{40}$$

Third, we perform a change of basis to absorb the oscillations induced by the vacuum Hamiltonian and in order to simultaneously diagonalize all remaining operators on the right-hand side of Eq. (37):

$$R_N^{(0)} \mapsto S^{(0)} = V_\alpha^\dagger R_N^{(0)} V_\alpha \,. \tag{41}$$

The derivation and explicit form of the x-independent unitary matrix V_α is given in Appendix A. It is of the form

$$V_\alpha = \begin{pmatrix} e^{i\alpha} f_{11} & e^{i\alpha} f_{12} \\ f_{21} & f_{22} \end{pmatrix} \,, \tag{42}$$

where f_{ij} are time-independent combinations of the absolute values of the matrix elements of $F^\dagger F$, and α denotes the phase of the matrix element $(F^\dagger F)_{12}$.

With this, Eq. (37) can be expressed as

$$\frac{\mathrm{d}S^0(x)}{\mathrm{d}x} = S^0(x)\left((i-\phi^{(0)})Y + x^2 D\right) - \left((i+\phi^{(0)})Y + x^2 D\right) S^0(x) + 2\phi^{(0)} Y \,, \tag{43}$$

where $Y = M_0/(T\,T_{\mathrm{EW}})\, V_\alpha^\dagger \langle V_N \rangle V_\alpha$ and D is defined in Appendix A. Both D and the diagonal matrix Y are x-independent. Equation (43) is moreover invariant under $F \leftrightarrow F^*$, i.e. in this basis, particles and anti-particles are described by the same quantity S^0 (to 0th order in μ_α). This makes this basis highly suitable for linearizing our system of differential equations. Note that the expressions for $R_N^{(0)}$ and $R_{\bar{N}}^{(0)}$ in the original basis however differ, as encoded in the transformation matrix $\bar{V}_\alpha(\alpha) = V_\alpha(-\alpha)$, see Eq. (42).

First order

We now turn to linearizing the full equation for $R_{N,\bar{N}}$ in this basis, see Eq. (41). To expand around the 0th order solution, we moreover change variables to

$$S_+ = S_N + S_{\bar{N}} = 2S^0 + \Delta S_+ \,, \quad S_- = S_N - S_{\bar{N}} = \Delta S_- \,, \tag{44}$$

where $S_{N,\bar{N}} = V_\alpha^\dagger(\pm\alpha) R_{N,\bar{N}} V_\alpha(\mp\alpha)$ and $\Delta S_\pm$ denote the contributions arising due to the presence of the terms proportional to μ_L in Eq. (27). With this,

$$\frac{d\Delta S_-}{dx} = -x^2[D, \Delta S_-] - i[Y, \Delta S_-] - \phi^{(0)}\{Y, \Delta S_-\} + \phi^{(1a)} O_\mu + \frac{\phi^{(1b)}}{2}\{O_\mu, S_0\} + \mathcal{O}(\mu_L \Delta S_-) \,, \tag{45}$$

with

$$\phi^{(1a)} \equiv -\frac{9\cdot 16\zeta(3)}{\pi^2 T}\gamma^{(1a)}$$
$$= \frac{1}{16\pi}\left[c_Q^{(1)}h_t^2 + c_{LPM}^{(1)} + (3g^2+g'^2)\left(c_V^{(1)} + \log\left(\frac{1}{3g^2+g'^2}\right)\right)\right], \tag{46}$$
$$\phi^{(1b)} \equiv -\frac{9\cdot 16\zeta(3)}{\pi^2 T}\gamma^{(1b)}$$
$$= \frac{1}{32\pi}\left[c_Q^{(2)}h_t^2 + c_{LPM}^{(2)} + (3g^2+g'^2)\left(c_V^{(2)} + \log\left(\frac{1}{3g^2+g'^2}\right)\right)\right], \tag{47}$$

and

$$O_\mu = \frac{1}{16}\frac{\pi^2}{9\xi(3)}\frac{M_0}{T_{EW}}V_\alpha^\dagger[F^\dagger\mu_L F + \Phi^* F^T \mu_L F^*\Phi]V_\alpha\,, \tag{48}$$

where $\Phi = \mathrm{diag}(\exp(-2i\alpha), 1)$.

Similarly, the equation for the asymmetry in the active sector can be cast as

$$\frac{16N_D T_{\rm EW}}{M_0}\frac{d\mu_{\Delta_\alpha}(x)}{dx} = \phi^{(1a)}(FF^\dagger)_{\alpha\alpha}\mu_{L_\alpha}(x) - \phi^{(0)}(FV_\alpha\Delta S_-(x)V_\alpha^\dagger F^\dagger)_{\alpha\alpha} \tag{49}$$
$$+\frac{\phi^{(1b)}}{2}(FV_\alpha S^0(x)V_\alpha^\dagger F^\dagger)_{\alpha\alpha}\mu_{L_\alpha}(x) + \mathcal{O}(\mu_L\times\Delta S)\,. \tag{50}$$

Note that the equation for ΔS_+ decouples from the equations for ΔS_- and μ at linear order. It is thus sufficient to solve Eqs. (43), (45) and (50). In total this enables a strong simplification of the system of differential equations, empowering a fast numerical solution and thus allowing to use this framework for a numerical scan of the parameter space.

The final asymmetries $Y_x = (n_x - n_{\bar{x}})/s$ are then obtained by evaluating the solutions of Eqs. (43), (45) and (50) at $T = T_{\rm EW}$:

$$Y_N = \frac{1}{s}\int\frac{d^3k_N}{(2\pi)^3}f_F^0(k_N)\mathrm{Tr}[\Delta R] = \frac{3}{8}\frac{45\zeta(3)}{\pi^4 g_s}\,\mathrm{Tr}[V_\alpha\Delta S_- V_\alpha^\dagger]\,, \tag{51}$$
$$Y_{B-L} = \frac{N_D}{s}\int\frac{d^3k_L}{(2\pi)^3}(f_L - f_{\bar{L}}) = -\frac{2N_D}{s}\mathrm{Tr}[\mu_\Delta]\int\frac{d^3k_L}{(2\pi)^3}f_F'(k_L/T) = \frac{45N_D}{12\pi^2 g_s}\mathrm{Tr}\mu_\Delta\,, \tag{52}$$
$$Y_B = \frac{28}{79}Y_{B-L}\,, \tag{53}$$

where $s = \frac{2\pi^2 g_s}{45}T^3$ is the entropy density. With Eq. (34), one immediately sees that $Y_N = Y_{B-L}$.

The time evolution of the above system is depicted in Fig. 1 for two benchmark points distinguished by the value of the Yukawa coupling F. The first benchmark, characterized by $|F| = 1.5\times 10^{-7}$, is essentially a weak washout scenario. Once the neutrino oscillations become effective, the asymmetries of both singlet and active sector grow monotonically until $T = T_{\rm EW}$ is reached. The second benchmark solution, given a higher value of the Yukawa coupling, $|F| = 1.4\times 10^{-6}$, shows the characteristic behavior of strong washout. After reaching a peak asymmetry of $\mathcal{O}(10^{-8})$ around $x \simeq 0.4$, the asymmetry is subsequently reduced by washout processes by about an order of magnitude. The final asymmetry is nevertheless sizable enough to comply with the observed value.

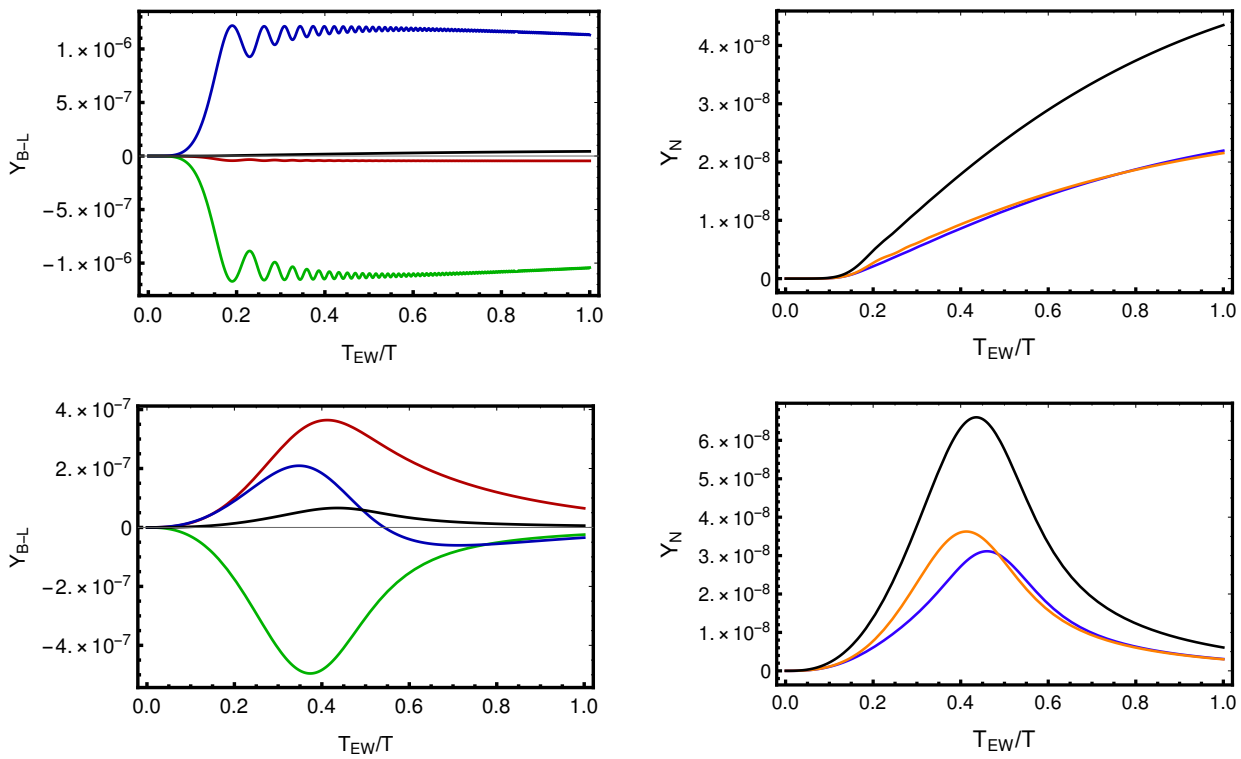

Figure 1: Asymmetries in the active and singlet sectors for different values of the Yukawa coupling $|F|$. **Left panel**: $B-L$ asymmetries in the three active flavors (colored) and total asymmetry (black). **Right panel**: asymmetries of the two singlet flavors (colored) and the total asymmetry (black). Since lepton number is conserved, the black curve in the left column identical to the black curve in the corresponding right panel. The values for the norm of the Yukawa coupling are (top to bottom) are $|F| = 1.5 \times 10^{-7}$ and 1.4×10^{-6}. Both examples fulfill all the low-energy neutrino constraints within the LSS-ISS setup.

4 Numerical analysis and results

In this section we perform a numerical analysis of the parameter space of the models presented in the Section 2, taking into account available constraints (discussed in Section 2.1) and requiring successful leptogenesis (Section 3). In the case of the LSS-ISS scenario, our results represent a direct extension of the analysis conducted in [17], which was limited to the weak washout regime. In contrast, our numerical study in this section is focused on the strong washout scenario. As already anticipated in [17], in this case the correct baryon asymmetry is obtained for relatively large mixing angles between the heavy and the active neutrinos, testable with future experiments such as NA62 [75], SHiP [76, 77], FCC-ee [78] and LBNF/DUNE [105]. We will then extend our analysis to the more refined models ISS(2,2) and ISS(2,3). Also in these cases our study will be focused on the strong washout regime since it was already found in [17] that viable leptogenesis cannot be achieved in the weak washout regime for these models. Although the two ISS setups feature a similar outcome in terms of allowed masses and mixing angles of the neutrinos responsible for the leptogenesis process, the ISS(2,3) receives additional constraints due to the presence of a potential DM candidate.

To ease the notation, we will refer to the mass scale of the pseudo-Dirac pair involved in leptogenesis as $m_{\rm PD}^2$, Δm^2 referring to the splitting between the two squared masses of this pair and $\Delta m \equiv \sqrt{\Delta m^2}$. If a second (heavier) pseudo-Dirac pair is present (as in the case of the ISS), we denote the corresponding mass scale as $M_{\rm PD}$.

4.1 The LSS-ISS model

To analyze our parameter space, we proceed in two steps. In the first one, we generate parameter points within the LSS-ISS neutrino mass model which reproduce the low-energy neutrino observables, i.e. the mass splittings and mixing angles observed in neutrino oscillations. We also impose the bounds from direct and indirect searches for singlet neutrinos discussed in Section 2.1. In a second step, we calculate the resulting baryon asymmetry, based on the differential equations given in Section 3. Here we briefly outline both procedures.

4.1.1 Parameter space

For the LSS-ISS case, we adopt the parametrization of Ref. [106]. For a normal-ordered hierarchy among the active neutrinos, the six Yukawa couplings in Eq. (5) are obtained as

$$Y_\alpha = \frac{y}{\sqrt{2}} \left[U_{\alpha 3}^{(\nu)\,*} \sqrt{1+\rho} + U_{\alpha 2}^{(\nu)\,*} \right] , \tag{54}$$

$$Y'_\alpha = \frac{y'}{\sqrt{2}} \left[U_{\alpha 3}^{(\nu)\,*} \sqrt{1+\rho} - U_{\alpha 2}^{(\nu)\,*} \right] + \frac{k}{2} Y_\alpha , \tag{55}$$

with $U^{(\nu)}_{\alpha i}$ denoting the entries of the 3×3 PMNS matrix[6] and

$$\rho \equiv \frac{\sqrt{1+r} - \sqrt{r}}{\sqrt{1+r} + \sqrt{r}}\,, \quad r \equiv \frac{|\Delta m^2_{\rm solar}|}{|\Delta m^2_{\rm atm}|}\,, \quad k \equiv \frac{\xi}{\epsilon}\,. \tag{56}$$

y and y' are two positive real parameters characterizing the size of the Yukawa couplings, which in the spirit of this model we will assume to be of similar size. In the case of an inverted hierarchy among the active neutrinos, one needs to replace

$$\rho \mapsto \frac{\sqrt{1+r} - 1}{\sqrt{1+r} + 1}\,, \quad U^{(\nu)}_{\alpha 3} \mapsto U^{(\nu)}_{\alpha 2}\,, \quad U^{(\nu)}_{\alpha 2} \mapsto U^{(\nu)}_{\alpha 1}\,. \tag{57}$$

This parametrization conveniently encodes the observed mixing angles in the PMNS matrix. Since one of the active neutrinos remains massless, we can directly associate the masses of the active neutrinos,

$$m_1 = 0\,, \quad m_2 = \left|\frac{\epsilon y y'(1-\rho)v^2}{2\Lambda}\right|\,, \quad m_3 = \left|\frac{\epsilon y y'(1+\rho)v^2}{2\Lambda}\right|\,, \tag{58}$$

with the measured mass splittings, eliminating a further parameter. The masses of the two heavy neutrinos are given by $m_{4,5} \simeq m_{\rm PD}(1 \mp \xi)$ with $m_{\rm PD} = |\Lambda|$. In this parametrization, the Dirac phase δ_{CP} and the Majorana phase $\alpha^{(\nu)}$ appear in Y and Y', whereas the third 'high-energy' phase is assigned to Λ.

With this we perform a systematic scan covering the parameter ranges

$$100 \text{ MeV} \leq m_{\rm PD} \leq 50 \text{ GeV}\,, \tag{59}$$

$$10^{-7} \leq y, y' \leq 10^{-4}\,, \tag{60}$$

$$10^{-7} \leq k \leq 1\,. \tag{61}$$

Here the range of Λ is bounded from below by the requirement that the singlet neutrinos should decay before BBN and from above by the assumption that the singlet neutrinos are ultra-relativistic, implying that lepton number is approximately conserved. The range of y and y' selects the strong washout regime ($|F| \gtrsim 10^{-7}$) where we omit too large Yukawa couplings since in this case the strong washout processes will erase all the previously produced asymmetry.[7] The range of k reflects that on the one hand, we expect ϵ and ξ to be of similar size (both violate lepton number by two units) while on the other hand, a mild hierarchy $\xi < \epsilon$ is preferred to simultaneously reproduce the light neutrino mass scale and obtain a sufficiently small mass splitting between the singlet states. Note

[6] Similar to the unitary matrix $\mathcal{U}$, the PMNS matrix $U^{(\nu)}$ is obtained by diagonalizing the neutrino mass matrix, however in this case after integrating out the SM singlet states.

[7] Note that within the framework of two heavy neutrinos and small LNV parameters presented here, we will typically obtain at most a moderate hierarchy between Yukawa couplings to different active flavors, $Y_e \sim Y_\mu \sim Y_\tau$. This provides a contrast to Ref. [16], where significant hierarchies were considered. This constraint does not apply to the hierarchy between the Yukawa couplings associated with the two different singlet states, which is governed by the parameter ϵ.

that the case $k \gg 1$ (and $k \ll \xi^2$) corresponds to the limit of the pure Inverse Seesaw, which will be discussed below.[8] For each parameter point the three CP phases are chosen randomly. All parameter points are furthermore checked for consistency with the bounds from direct and indirect searches for singlet neutrinos discussed in Section 2.1.

Considering the parameters relevant for leptogenesis, the choice of small LNV parameters ϵ and ξ has interesting consequences for the matrix V_α introduced in Eq. (42). Recall that V_α is the unitary matrix diagonalizing the operators in the 0th order differential equation for the singlet neutrinos, i.e. diagonalizing $F^\dagger F$. Let us investigate the properties of V_α in a toy model with a single active neutrino, where the neutrino mass matrix is given by Eq. (6). In the limit where $\epsilon, \xi \to 0$, the matrix $\mathcal{U}$ diagonalizing the symmetric matrix $\mathcal{M}^{(\nu)}$, $\mathcal{U}^T \mathcal{M}^{(\nu)} \mathcal{U} = m_{\text{diag}}$, is given by[9]

$$\mathcal{U} = \begin{pmatrix} 1 & 0 & 0 \\ 0 & ie^{i\beta/2}/\sqrt{2} & e^{-i\beta/2}/\sqrt{2} \\ 0 & -i/\sqrt{2} & 1/\sqrt{2} \end{pmatrix} . \tag{62}$$

Here β is the phase of Y', whereas Y can be taken to be real and positive without loss of generality. The columns of $\mathcal{U}$ are the eigenvectors of $(\mathcal{M}^{(\nu)})^\dagger \mathcal{M}^{(\nu)}$, and the requirement of $m_{\text{diag}} > 0$ determines the phase of these vectors (up to an ambiguous unphysical sign). With this, we can determine the Yukawa couplings in the mass eigenbasis as

$$F^{\alpha I} = Y_{\alpha j} \mathcal{U}_{jI} = e^{-i\beta/2} Y/\sqrt{2}\,(\pm i\,,\ \pm 1)\,. \tag{63}$$

We can now determine the unitary matrix V_α which diagonalizes $F^\dagger F$. Parameterizing V_α as

$$V_\alpha = \begin{pmatrix} -e^{i\alpha}\cos\theta & e^{i\alpha}\sin\theta \\ \sin\theta & \cos\theta \end{pmatrix} , \tag{64}$$

we can immediately identify $\alpha = \pi/2$ and $\theta = \pi/4$. Thus, in the limit of vanishing LNV parameters, the eigenvectors of the effective potential V_N are maximally mixed combinations of the degenerate mass eigenstates, and the associated CP-phase indicates maximal CP-violation; the two Majorana states pair form a massive Dirac particle. The same conclusion can be shown to hold in the full model with 3 active neutrino species.

Switching on ϵ and ξ in the full model with 3 active neutrino species enables a deviation from the above results $\alpha = \pi/2$ and $\theta = \pi/4$. However, we stress that for small LNV parameters, values

[8] Swapping the labels of the fourth and fifth column in the mass matrix corresponds to $\epsilon \mapsto 1/\epsilon$, i.e. $k \to \xi^2/k$. In this sense, $k \ll \xi^2$ also corresponds to the pure ISS limit.

[9] In the limit $\epsilon = \xi = 0$, $\mathcal{M}^{(\nu)}$ has two degenerate eigenvalues and $\mathcal{U}$ is not unique. The solution presented here is distinguished since it continuously maps to the solution for small but finite ϵ and ξ.

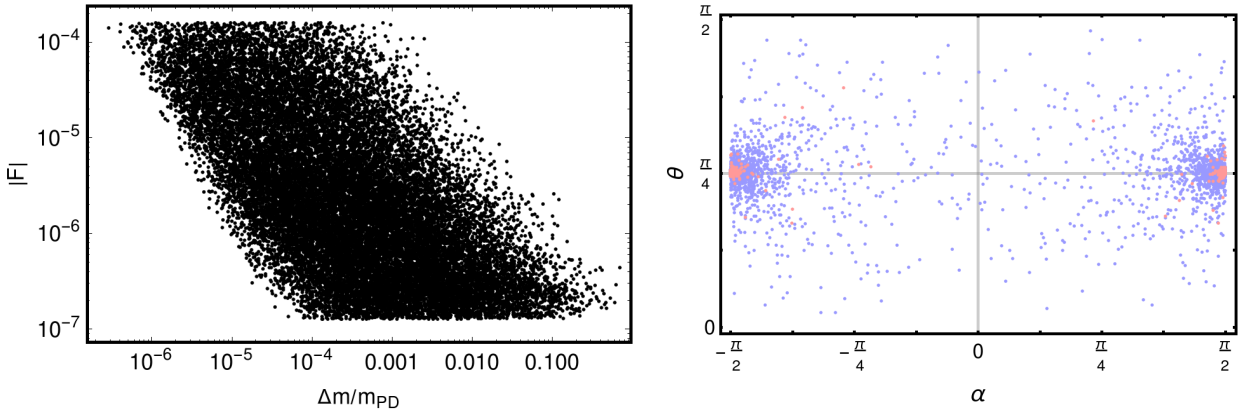

Figure 2: Characteristic properties of the relevant parameter space in the LSS-ISS model. **Left panel:** Norm of the 2×3 Yukawa matrix compared to the relative mass splitting. **Right panel:** The mixing angle θ and the CP-violating phase α describe the transition from the mass eigenbasis to the eigenbasis of the effective potential for the singlet neutrinos. For small LNV parameters, these are pushed to $\alpha \simeq \pm\pi/2$ and $\theta \simeq \pi/4$. In the right panel, we distinguish between normal hierarchy (blue) and inverted hierarchy (red) in active neutrino mass spectrum. Quantities insensitive to this distinction (as in the left panel) are shown in black.

of $\alpha \simeq \pi/2$ and $\theta \simeq \pi/4$ are the generic expectation. To avoid entering into too fine-tuned regions of the parameter space, we will thus impose the additional restriction that α and θ must lie within 10% of the values derived above.

In Fig. 2 we demonstrate some of the key properties of this parameter space, focusing on the parameters which will be relevant for leptogenesis. In the left panel, we show the dependence of the overall scale[10] of the Yukawa coupling on the relative mass splitting between the two heavy neutrinos. Small relative mass splittings, which render leptogenesis through neutrino oscillations particularly efficient, are obtained for large Yukawa couplings - this emphasizes why the strong washout regime is of particular interest for this scenario. The depicted dependence can be easily understood from Eq. (10): The ratio $|F|^2/m_{\rm PD} \simeq |Y|^2/\Lambda$ is fixed by the light neutrino mass up to a factor of ϵ (for $k < 1$). The relative mass splitting above the EW phase transition is determined by ξ, leading to $|F| \simeq \sqrt{2\,k\,m_\nu\,m_{\rm PD}}/(v\Delta m/m_{\rm PD})$. Taking into account the ranges of k and $m_{\rm PD}$ in Eqs. (59) and (61), this explains the depicted relation between $|F|$ and $\Delta m/m_{\rm PD}$. Finally, the right panel of Fig. 2 illustrates how for small LNV parameters, the parameters of the mixing matrix in the heavy neutrino sector are pushed to $\alpha \simeq \pm\pi/2$ and $\theta \simeq \pi/4$. This effect is especially pronounced in the case of the inverted hierarchy.

Additional singlet neutrinos may lead to observable effects not only in direct and indirect searches (described in Section 2.1) and in leptogenesis (described below), but also in neutrinoless double beta decay. Notice however that the contribution to the neutrinoless effective mass $m_{0\nu\beta\beta}$

[10]Here we define $|F|$ (norm of F) as the largest singular value of the matrix F.

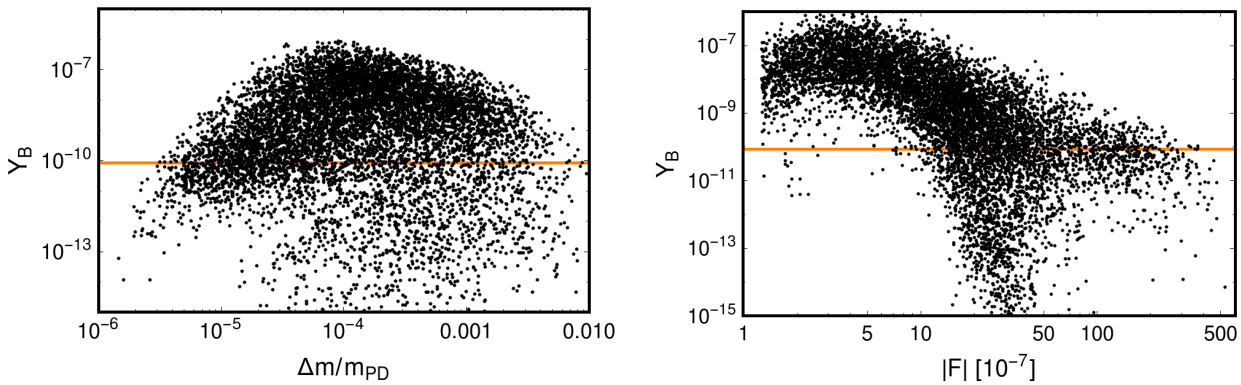

Figure 3: Dependence of the generated baryon asymmetry on the mass splitting and on the norm of the Yukawa couplings in the LSS-ISS model. The horizontal orange line denotes the observed baryon asymmetry, $Y_B = 8.6 \times 10^{-11}$ [111].

from a pseudo-Dirac pair is characterized by two terms which are similar in modulus but opposite in sign (see Eqs. (2) and (62)), with an exact cancellation realized in the limit of vanishing LNV parameters (when the pseudo-Dirac pair reduces to a lepton number conserving Dirac state). For that reason, in the LSS-ISS setup discussed in this paper, we find no significant enhancement of the SM contribution to neutrinoless double beta decay in any part of the parameter space; see also the discussions in Refs. [22, 107, 108, 108, 109].[11]

4.1.2 Leptogenesis in the LSS-ISS

We now turn to the baryon asymmetry in this model, implementing the procedure described in Section 3. In particular, we numerically simultaneously solve the differential equations (43), (45) and (50), starting from vanishing abundances of the singlet neutrinos at $x = 0.5 \times 10^{-3}$ and then evolving the system until the EW phase transition at $x = 1$. We stress that the simplifications discussed in Section 3 are crucial to speed up the numerical computation, which can now easily be performed on an ordinary desktop computer.

In Fig. 3 we show the resulting asymmetry as a function of the relative mass splitting and of the norm of the 2×3 Yukawa matrix. We find a preference for a relative mass splitting around $\Delta m/m_{\rm PD} \sim 10^{-4} - 10^{-3}$ and for $|F| \lesssim 10^{-5}$. Larger relative mass splittings render leptogenesis through neutrino oscillations inefficient. Smaller relative mass splittings come with larger Yukawa

[11] Ref. [14] recently pointed out that an enhancement of the $0\nu\beta\beta$ decay rate due to two additional heavy neutrinos can be achieved in a specific corner of the parameter space, characterized by relatively small $m_{\rm PD}$, large Δm and very different mixings of the two heavy neutrinos to ν_e. Moreover, note that under the addition of three singlet neutrinos, successful leptogenesis via neutrino oscillation and a sizable enhancement of the neutrinoless double beta decay rate are simultaneously possible [109]. This can be traced back to the observation that in the case of three singlet neutrinos, leptogenesis is possible without a high degree of mass degeneracy [14]. While this is surely a very attractive scenario, in this case the connection to (small) LNV is lost. See also [18, 110] for related analyses.

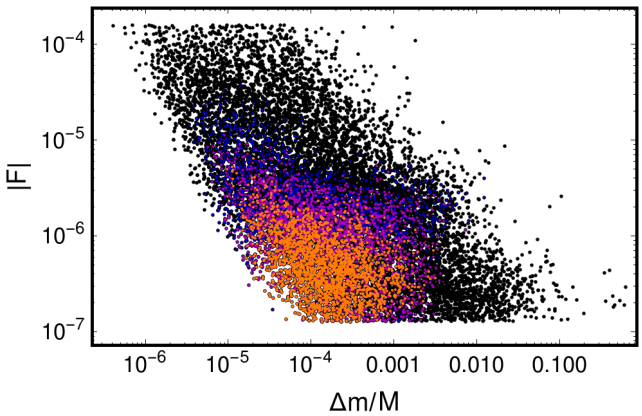

Figure 4: Generated baryon asymmetry in the LSS-ISS model in terms of the relative mass splitting in the heavy neutrino pair and the norm of the corresponding Yukawa couplings. The orange (purple, blue) points mark values of the asymmetry larger than 10^{-8} ($10^{-9}, 10^{-10}$).

couplings (see Fig. 2), resulting in a too efficient washout of the generated asymmetry before the EW phase transition. These results confirm that the parameter ranges specified above indeed cover all the parameter space relevant for leptogenesis in the strong washout regime.

These results are further emphasized in Fig. 4, where the different colours indicate the level of asymmetry achieved in different parts of the parameter space. The depicted region is bounded to the bottom left by the lower bound on k and $m_{\rm PD}$ in Eqs. (59) and (61), see Fig. 2. To the right, the relative mass splitting becomes too large to yield effective leptogenesis, whereas from above, too large Yukawa couplings impose a too strong washout of the generated asymmetry.

In Fig. 5 we depict the mixing between the active and the singlet sector as a function of the heavy neutrino mass scale - for the parameter points which yield successful leptogenesis. Here we consider any parameter point leading to $|Y_B| > Y_B^{\rm obs}$ as a viable parameter point for leptogenesis, since for any given parameter point, we can always modify the phases $\delta_{\rm CP}$, $\alpha^{(\nu)}$ and $\arg(\Lambda)$ to reduce the asymmetry ($Y_B \to 0$ if the CP-violating phases vanish) or to flip its sign. This mixing is parametrized by the corresponding element $\mathcal{U}_{\alpha I}$ in the unitary matrix $\mathcal{U}$ which diagonalizes the total neutrino mass matrix $\mathcal{M}^{(\nu)}$. Here we show the mixing between the lightest of the singlet neutrinos ($I = 4$) and the electron ($\alpha = e$) / muon ($\alpha = \mu$) neutrino. For comparison we show the reach of future experiments such as NA62 [112], SHiP [76, 77], FCC-ee [78] and LBNF/DUNE [79]. We note that a sizable part of the parameter space can be probed by these experiments, in agreement with earlier studies, see e.g. [27, 113]. This result is in contrast with what was found in the case of the weak washout regime in [17], where the mixing angle were found to be too small to be probed experimentally. Upcoming experiments hence have the potential to discriminate between the weak and strong washout regimes in the context of the LSS-ISS model.

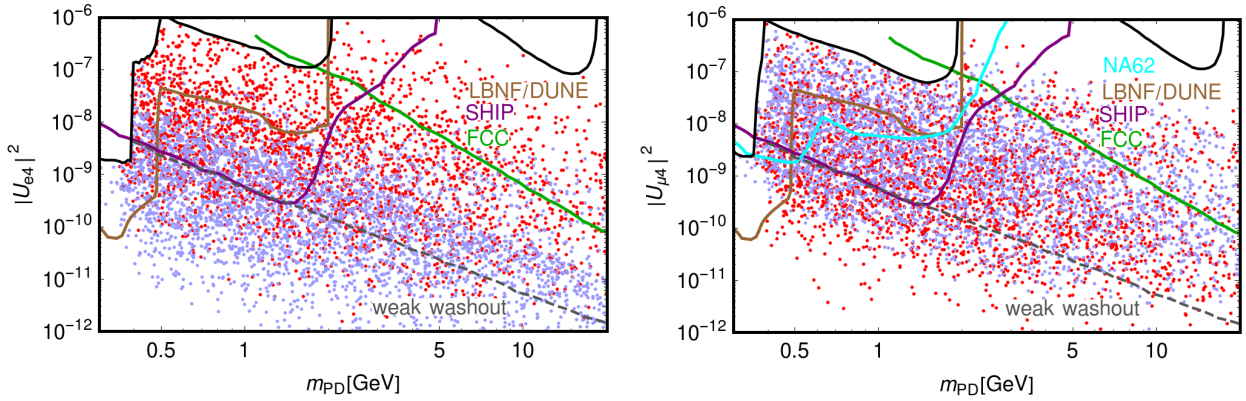

Figure 5: Mixing between the active and singlet neutrino sector in the LSS-ISS model for viable leptogenesis solutions. The black line denotes the existing bounds discussed in Section 2.1, the colored lines refer to the sensitivity curves of the planned experiments NA62, LBNF/DUNE, FCC-ee and SHiP. For comparison, the dashed gray line indicates the largest mixing found in the weak washout regime in Ref. [17]. As in Fig. 2, the blue (red) points correspond to normal (inverted) hierarchy. The difference between inverted and normal hierarchy is most evident in the mixing with the electron neutrino, here the inverted hierarchy leads to a significantly larger mixing.

4.2 The Inverse Seesaw

4.2.1 Parameter space

To perform the numerical exploration of the parameter space of the minimal Inverse Seesaw models discussed in Sec. 2.3 we adopt a parametrization inspired by the Casas-Ibarra one [114], but adapted for the ISS(2,2) and ISS (2,3) models. In the framework of a generic ISS mechanism, the low-energy effective neutrino mass matrix m_ν is given by the relation

$$d\left(n^{-1}\right)^T \xi\,\Lambda\left(n^{-1}\right) d^T = m_\nu = U^* \hat{m}_\nu U^\dagger, \tag{65}$$

where $\hat{m}_\nu$ is a diagonal matrix containing the physical neutrino masses and U is a unitary matrix, which approximately coincides with the PMNS mixing matrix $U^{(\nu)}$ measured in experiments.[12] By working in a basis in which the sub-matrix $\xi\,\Lambda$ in Eq. (12) is real and diagonal, it is possible to rewrite Eq. (65) as

$$\underbrace{U^T d\left(n^{-1}\right)^T \sqrt{\xi\,\Lambda}}_{K}\,\underbrace{\sqrt{\xi\,\Lambda}\left(n^{-1}\right) d^T U}_{K^T} = \hat{m}_\nu, \tag{67}$$

where we have defined a complex (3×2)-dimensional matrix K. The relation $\sum_{i=1,2} K_{\alpha i} K_{\beta i} = \delta_{\alpha\beta} m_\alpha$, with the additional constraint $m_\alpha = 0$ for $\alpha = 1$ ($\alpha = 3$) for normal (inverted) hierarchy

[12] The two matrices are related by

$$U^{(\nu)} = \left(1 - \frac{1}{2}\Theta\Theta^\dagger\right) U + \mathcal{O}(\Theta^3), \tag{66}$$

where the matrix Θ parametrizes the deviation from unitarity of the PMNS matrix. Given the strong experimental constraints on it, Θ can be neglected in the present discussion.

(we recall that in the ISS (2,2) and (2,3) models, the lightest neutrino is massless) provides 10 independent conditions for the entries in K, leaving only 2 free parameters. Consequently the matrix K can be parametrized as

$$K_{N,I} = \sqrt{\hat{m}_\nu}\, R_{N,I}, \tag{68}$$

where the "orthogonal" matrix R reads

$$R_N = \begin{pmatrix} 0 & 0 \\ \cos\gamma & \sin\gamma \\ -\sin\gamma & \cos\gamma \end{pmatrix}, \quad R_I = \begin{pmatrix} \cos\gamma & \sin\gamma \\ -\sin\gamma & \cos\gamma \\ 0 & 0 \end{pmatrix}, \tag{69}$$

for normal and inverted hierarchy, respectively, and where γ is a complex angle. By inverting the definition for K in Eq. (67), it is possible to parametrize the Dirac (and hence the Yukawa) matrix d as

$$d_{(2,2)} = U^* \sqrt{\hat{m}_\nu}\, R_{N,I} \sqrt{(\xi\,\Lambda)^{-1}} n^T. \tag{70}$$

Equations (68-69) ensure the relation in Eq. (67) to hold for arbitrary values of γ. However, the imaginary part of γ cannot be too large, since in the present parametrization the Yukawa couplings are linearly proportional to the functions $\cos\gamma$ and $\sin\gamma$, and large Yukawa entries can violate the perturbativity of couplings, or the seesaw condition $||d|| << ||n||$ (interpreted as a condition on the magnitude of the entries in the d and n matrices, see Eq. (12)), rendering in either case the relation in Eq. (65) not suitable to account for low energy phenomenology in neutrino experiments. We thus conduct our scan in the range

$$0 \leq \rho \leq 2\pi, \qquad 0 \leq \phi \leq 2\pi, \qquad \text{with } \gamma = \rho e^{i\phi}, \tag{71}$$

and we perform a consistency check on each realization of the model, explicitly diagonalizing the full (7×7) mass matrices constructed with the present parametrization, and verifying their agreement with neutrino data.

For the (2,3) ISS model an analogous parametrization can be derived: in this case, however, since n is not squared the matrix n^{-1} is not well defined, and a more general version of Eq. (65) holds:

$$d\ a\ d^T = m_\nu = U^* \hat{m}_\nu U^\dagger, \tag{72}$$

where a is the (2×2)-dimensional submatrix defined as

$$M^{-1} = \begin{pmatrix} a_{2\times 2} & \cdots \\ \vdots & \ddots \end{pmatrix}, \qquad \text{with } M = \begin{pmatrix} 0 & n \\ n^T & \xi\,\Lambda \end{pmatrix}. \tag{73}$$

By diagonalizing a with the help of a unitary matrix W, $a = W^* \hat{a} W^\dagger$, we obtain

$$\underbrace{U^T d\, W^* \sqrt{\hat{a}}}_{K_{(2,3)}} \underbrace{\sqrt{\hat{a}}\, W^\dagger d^T U}_{K^T_{(2,3)}} = \hat{m}_\nu, \tag{74}$$

from which, analogously to the derivation of eq. (70), we can write

$$d_{(2,3)} = U^* \sqrt{\hat{m}_\nu}\; R_{N,I} \sqrt{\hat{a}^{-1}}\; W^T. \tag{75}$$

To efficiently explore the full parameter space of interest we perform a grid-based numerical scan: for each phenomenologically relevant parameter in the model we chose physically motivated upper and lower bounds, and divide the resulting interval in a number of steps, equally distributed on a logarithmic scale.

The mass scales of the model can be easily linked to the order of magnitude of the sub-matrices in the full ISS mass matrix: the first (second) row of the submatrix n determines the mass scale for the lightest (heavier) pseudo-Dirac pair, while the submatrix $\xi\,\Lambda$ determines the mass splittings within the pseudo-Dirac states, as well as the mass scale for the lightest sterile state in the ISS(2,3). For each point in the sampling of the parameter space of the model, we fix a value for each of these three parameters and generate, in the corresponding sub-matrices, random entries; these entries are of the same order of magnitude than the reference parameter in the scan of the ISS(2,2). As will be discussed extensively in the following, the ISS(2,3) requires a certain amount of hierarchy in the entries of the submatrix n in order to accommodate viable active neutrino-DM mixing angles; we will thus consider, in its scan, random entries that span up to 3 orders of magnitude around the reference parameter. Once the sub-matrices n and $\xi\,\Lambda$ are generated in this way, the submatrix d is determined following Eqs. (70) or (75). We scan over the following range of masses:

$$\begin{aligned} m_{\rm PD} &\in [0.1 - 40]\ \text{GeV}, \\ M_{\rm PD} &\in \left[125 - 10^6\right]\ \text{GeV}, \\ m_{\rm DM} &\in [0.1 - 50]\ \text{keV}, \end{aligned} \tag{76}$$

where m_{PD} (M_{PD}) represent the mass of the lightest (heavier) pseudo-Dirac pair and $m_{DM} \simeq \Delta m$ corresponds to mass splitting in the pairs, or equivalently the mass of the DM candidate in the ISS(2,3). Here the range of $m_{\rm PD}$ is determined as in Eq. (59), while $M_{\rm PD}$ is bounded from above by the perturbative unitarity condition, see Eq. (1), and from below by requiring that the generated lepton asymmetry is not washed out by the heavier pseudo-Dirac pair (see below). Finally for the intermediate scale $m_{\rm DM}$, we concentrate on the viable mass range for sterile neutrino DM found in Ref. [23].

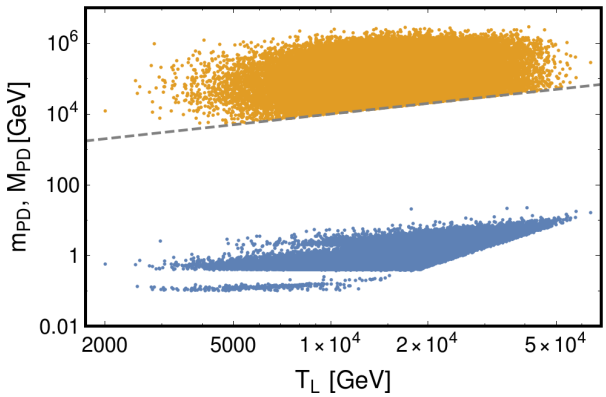

Figure 6: Mass scales for the lighter (blue) and heavier (orange) pseudo-Dirac pair in the ISS(2,2) as a function of the leptogenesis temperature T_L. Orange points below the dashed line $T_L = M_{PD}$ would lead to a too strong washout of the generated asymmetry.

4.2.2 Leptogenesis in the ISS(2,2)

Ref. [17] demonstrated that the minimal ISS models are not capable of reproducing the observed baryon abundance in the weak washout regime. This can be understood by considering a toy model with one active flavor and one heavy pseudo-Dirac pair with mass scale $m_{\rm PD}$ and mass splitting Δm. In this case, the mass scale of the active neutrino and the mass splitting within the pseudo-Dirac pair are given by Eqs. (14) and (15), implying a relative mass splitting of

$$\frac{\Delta m}{m_{\rm PD}} \simeq 0.6 \left(\frac{10^{-7}}{|F|}\right) \left(\frac{m_{\rm PD}}{\rm GeV}\right)^{1/2} \left(\frac{m_\nu}{0.05\ \rm eV}\right)^{1/2} . \tag{77}$$

In the weak washout regime, $|F| \lesssim 10^{-7}$, this is much larger than mass splitting $\Delta m/m_{\rm PD} \sim 10^{-6} - 10^{-2}$ required for successful leptogenesis, see Fig. 3. Ref. [17] generalized this argument to realistic models of more active and singlet neutrino flavors, confirming the above naive reasoning also in these cases. However, Eq. (77) also illustrates that these difficulties may be overcome in the strong washout regime with $|F| \gg 10^{-7}$. In this section we demonstrate how indeed low-scale leptogenesis can be successfully implemented within the minimal realistic ISS framework.

The minimal ISS mechanism which can reproduce the observed neutrino masses and mixings is the ISS(2,2), containing two additional pairs of pseudo-Dirac neutrinos [22]. In this section we focus on the possibility that the lighter pseudo-Dirac pair generates the lepton asymmetry as described in Section 3, whereas the mass scale of the second pseudo-Dirac pair is taken to be much heavier, so that it effectively decouples during leptogenesis. This will set the stage for the following section, where in the context of the ISS(2,3), we consider the possibility of simultaneously accounting for (a fraction of) dark matter in the form of sterile neutrinos. We point out that one could also consider the case in which the generation of the baryon asymmetry is accounted by only the heavier pseudo-Dirac pair or by both pairs. We postpone the discussion of these cases to a future study.

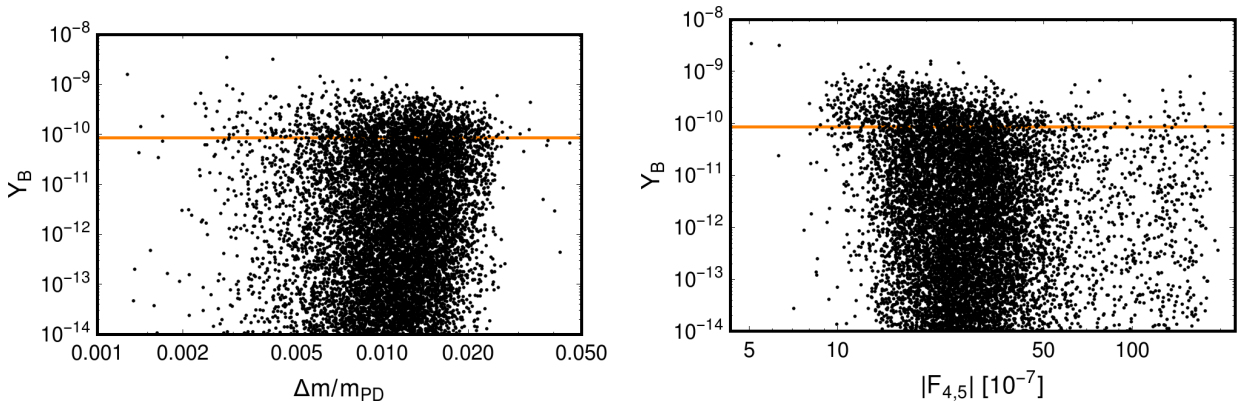

Figure 7: Dependence of the produced baryon asymmetry in the ISS(2,2) on the mass splitting and on the magnitude of the Yukawa couplings of the lighter pseudo-Dirac pair. The horizontal orange line indicates the observed asymmetry.

Focusing on leptogenesis through the lighter pseudo-Dirac pair requires nevertheless control over the washout rates induced by the heavier pair. Typically, the heavier pair will come with larger Yukawa couplings, thus thermalizing earlier, and its interactions with the SM thermal bath can wash out any asymmetry generated by the lighter pair. If however the heavier pair is non-relativistic, its abundance and accordingly the washout processes are exponentially Boltzmann suppressed. Specifically, we will require that at the characteristic leptogenesis temperature T_L (representing in good approximation the temperature at which most of the asymmetry is produced, even if eventually depleted by washout at later times (see also Appendix A)),

$$T_L = \left(\frac{\pi^2}{54\,\zeta(3)} M_0\, m_{PD}\, \Delta m \right)^{1/3} , \tag{78}$$

the number density of the lighter pair is larger than that of the heavier one,

$$1 \geq \max\{R_N^{11}, R_N^{22}\} > \exp(-M_{PD}/T) \quad \text{at } T = T_L\,. \tag{79}$$

In Fig. 6 we show the masses of the heavier pair (in orange) and of the lighter pair (in blue) in terms of the corresponding leptogenesis temperature T_L. The dashed line denotes $T_L = M_{PD}$, orange points below this line will not obey Eq. (79). This sets the lower bound for the range of M_{PD} in Eq. (76).

Restricting ourselves to points which do obey the condition (79) and for which the washout due to the heavier pair is thus negligible, we proceed as in Section 4.1.2 to calculate the resulting baryon asymmetry, applying the formalism of Section 3 to the lighter pseudo-Dirac pair. In Fig. 7 we show the resulting asymmetry as a function of the mass splitting and the Yukawa coupling. Compared to the LSS-ISS model of Fig. 3, we note that the mass splitting and the Yukawa couplings are pushed to larger values, reducing the generated asymmetry. While we still find points which produce a sufficient amount of baryon asymmetry, this is more difficult than in the LSS-ISS case. This is the

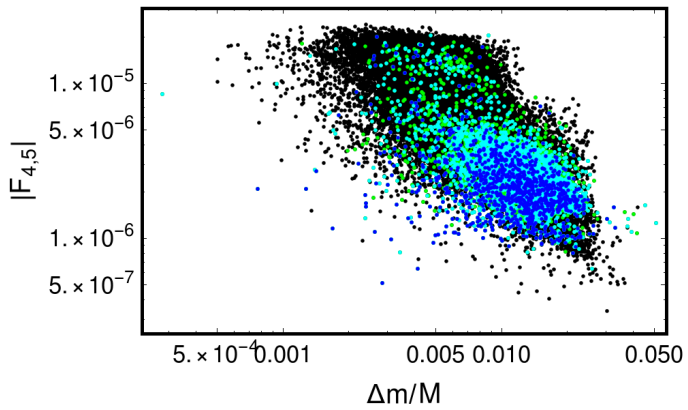

Figure 8: Generated baryon asymmetry in the IS(2,2) in terms of the relative mass splitting in the lighter pseudo-Dirac neutrino pair and the absolute value of the corresponding Yukawa coupling. The blue (cyan, green) points mark values of the asymmetry larger than 10^{-10} ($10^{-11}, 10^{-12}$).

result of the restriction schematically given by Eq. (77) together with the observation that too large Yukawa couplings lead to a too strong washout. Figure 8 summarizes these results in the Yukawa coupling versus mass-splitting plane.

As a result of this tension (Eq. (77) prefers $|F| \gg 10^{-6}$, the preferred range for leptogenesis is $10^{-7} < |F| < 5 \cdot 10^{-6}$), we find a preference for parameter points which feature a (mildly) hierarchical Yukawa spectrum with respect to the active flavor index α. A typical example of this type is depicted in Fig. 9. While the Yukawa coupling to the τ-flavor is relatively large, well in the strong washout regime, the coupling to the μ-flavor is much smaller, experiencing only marginal washout (green curve in the left panel). Since the total asymmetry summed over both sectors always vanishes, the asymmetry stored in the active μ-flavor induces asymmetries in the singlet flavors as well as in the other active flavors. This is similar to the situation in flavored leptogenesis [14]. For the parameter point depicted in Fig. 9, we find a mass splitting of $\Delta m/m_{PD} \simeq 0.01$ and an asymmetry of $|Y_B| \simeq 5.7 \cdot 10^{-10}$.

In analogy with Fig. 5, Fig. 10 illustrates the mixing between the lighter pseudo-Dirac pair and the active sector, compared to the corresponding expected sensitivities of NA62, LBNF/DUNE, FCC-ee and SHiP (the heavier pseudo-Dirac pair is not visible in these experiments). Notice that, since the region of viable leptogenesis in the ISS covers a smaller range of masses and mixings with respect to the LSS-ISS case, future experiments can probe almost the all of this space. The lower abundance of points associated with the inverted hierarchy is due to the observation that the ISS setup for neutrino mass generations generally disfavors the inverted hierarchy [22].

The effective mass in the amplitude of neutrinoless double beta decay, see Eq. (2), is shown in Fig. 11. Contrary to the LSS-ISS model, the ISS framework in principle allows for the possibility of sizable contributions, detectable in upcoming experiments [22]. However we do not observe this enhancement here for several reasons: firstly, for the contribution of the pseudo-Dirac pairs, an

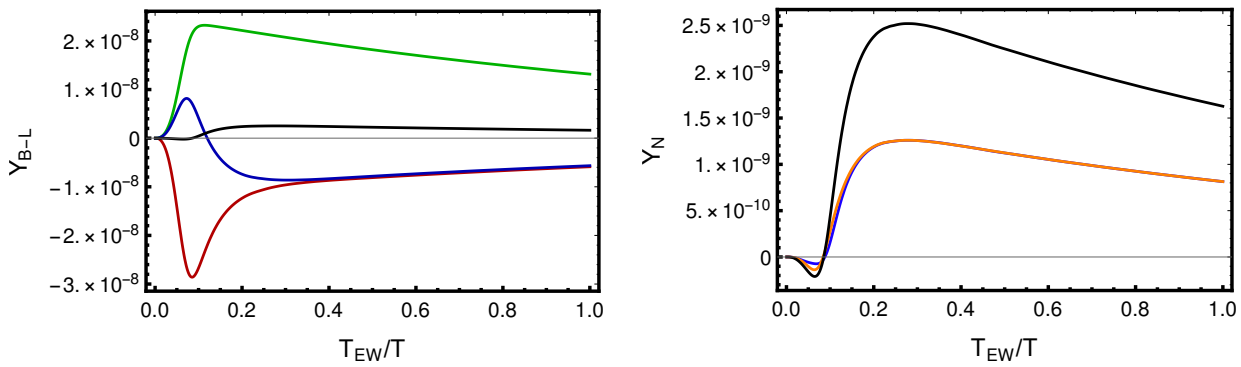

Figure 9: Asymmetries in the active and singlet sector in the ISS(2,2), here for an example with a sizable hierarchy in the Yukawa couplings $|F|$, $|F_{\tau,i}| \simeq 1.2 \cdot 10^{-6} > |F_{e,i}| \gg |F_{\mu,i}| \simeq 1.2 \cdot 10^{-7}$. **Left panel:** $B-L$ asymmetries in the active flavors e, μ, τ (red, green, blue) and total asymmetry (black). **Right panel:** asymmetries in the two sterile flavors of the lighter pseudo-Dirac pair (colored) and the total asymmetry (black). For this parameter point, the total baryon asymmetry is found to be $|Y_B| = 5.7 \cdot 10^{-10}$.

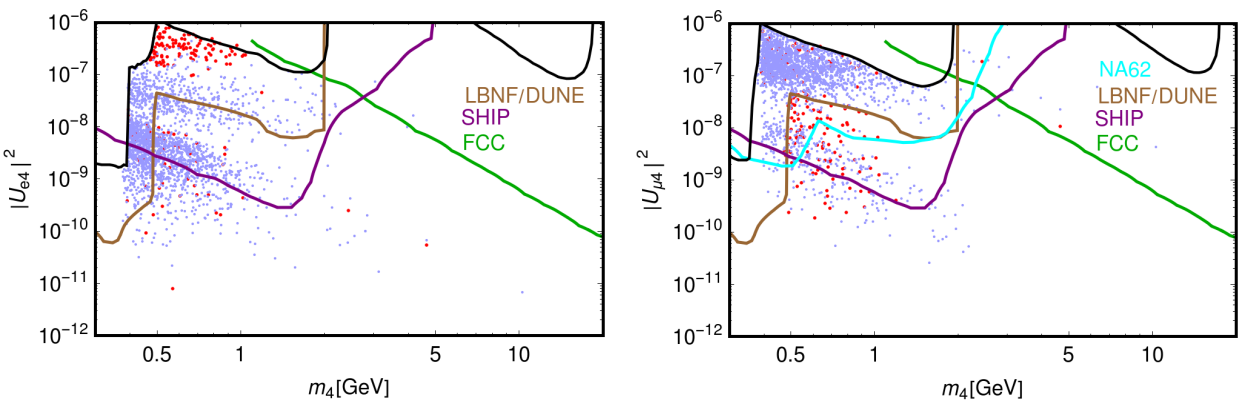

Figure 10: Mixing between active and singlet neutrino sector in the ISS(2,2) for viable leptogenesis solutions. The black line denotes the existing bounds discussed in Section 2.1, the colored lines refer to the sensitivity curves of the planned future experiments NA62, LBNF/DUNE, FCC-ee and SHiP. Solutions corresponding to the normal (inverted) hierarchy are shown in blue (red).

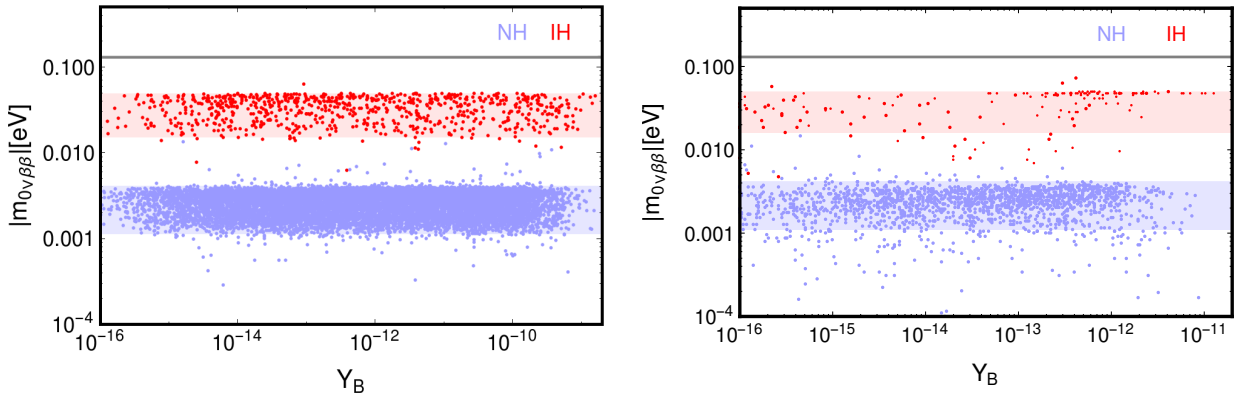

Figure 11: Effective mass parameter of neutrinoless double beta decay in the ISS(2,2) (left panel) and ISS(2,3) (right panel) in terms of the generated baryon asymmetry. Blue (red) points denote solutions corresponding to the normal (inverted) hierarchy. The shaded bands denote the corresponding SM contributions, the horizontal line the current experimental upper bound [82, 83]. In the right panel, the condition of a cosmologically viable DM abundance has been imposed.

analogous cancellation to the one already discussed in the framework of the LSS-ISS model is at play. In addition the Inverse Seesaw strongly prefers a normal ordering for the light neutrinos, which, together with a massless state, results in the minimal possible contribution of active neutrinos to the effective mass $m_{0\nu\beta\beta}$. In the ISS(2,3) the contribution of the isolated light sterile state could be sizable, however cosmological constraints strongly limit the allowed values for its mixing with the active sector (see Sec. 4.2.3) in the keV mass range, resulting again in a suppressed contribution to $m_{0\nu\beta\beta}$.

4.2.3 Leptogenesis and dark matter in the ISS(2,3)

Having established that the Inverse Seesaw mechanism can account for a neutrino spectrum suitable for leptogenesis, while simultaneously agreeing with all low-energy neutrino data, we now turn to the question if the Inverse Seesaw mechanism can (simultaneously) account for dark matter in the form of sterile neutrinos. To this end, we consider the minimal ISS realization which can account for the low-energy neutrino data and also provides a dark matter candidate, the ISS(2,3), see Sec. 2.3. Here the ISS(2,2) mass spectrum is extended by an additional, mostly sterile state at an intermediate mass scale which can constitute (a fraction of) dark matter [22]. The mass of this state is directly linked to the mass splitting within the lighter pseudo-Dirac pair, which is one of the key parameters determining the generated baryon asymmetry. For what concerns the analysis of the viable parameter space for leptogenesis, the ISS(2,3) closely resembles the ISS(2,2) model of the previous sections. Here we hence focus on the role played by the additional intermediate scale sterile state.

Any stable new physics neutrino state with a non-vanishing mixing to the active neutrinos

will be produced through active - sterile neutrino conversions according to the so-called Dodelson - Widrow (DW) mechanism [115]. The resulting abundance is proportional to the active-sterile mixing and can be expressed as [116, 117]:

$$\begin{aligned}\Omega_{\rm DM}h^2 &= 1.1\cdot 10^7 \sum_\alpha C_\alpha(m_{\rm DM})\,|\mathcal{U}_{\alpha 4}|^2 \left(\frac{m_{\rm DM}}{\rm keV}\right)^2 , \quad \alpha = e,\mu,\tau \\ &\simeq 0.3 \left(\frac{\sin^2 2\theta_{\rm DM}}{10^{-8}}\right)\left(\frac{m_{\rm DM}}{10\,{\rm keV}}\right)^2 . \end{aligned} \tag{80}$$

where the coefficients C_α can be determined numerically and are found to be of order 0.5 [116]. Here $\mathcal{U}$ is the unitary mixing matrix introduced below Eq. (18) and $\mathcal{U}_{\alpha 4}$ parametrizes the mixing between the DM candidate and the active sector, $\sin^2 2\theta_{\rm DM} = 4\sum_{\alpha=e,\mu,\tau}|\mathcal{U}_{\alpha 4}|^2$.

The range of viable DM masses is restricted to $0.1\,{\rm keV} \lesssim m_{\rm DM} \lesssim 50\,{\rm keV}$. Smaller masses are forbidden by the Tremain-Gunn bound [118] (derived by comparing the observed size of dwarf galaxies with a Fermi sphere of DM fermions, see also [119, 120]) while above 50 keV, the DM candidate is no longer cosmologically stable. Taking into account additional observational constraints on the active sterile mixing, the DW mechanism can account for about 30% of the total dark matter density today [22]. In particular, to avoid overproduction of dark matter, the active-sterile mixing angle is required be very small, $\sin^2 2\theta_{\rm DM} < 10^{-(7\div 10)}$.

The generic value of the active-sterile mixing is given by $\sin^2 2\theta_{\rm DM} = \mathcal{O}(Y^2v^2/\Lambda^2)$, leading to an overproduction of DM in a wide range of the parameter space. This mixing angle is however suppressed if the entries of the submatrix n in Eq. (12) feature a significant hierarchy, see appendix B. This is illustrated in the left panel of Fig. 12. Here the yellow points avoid the overproduction of dark matter, typically requiring a hierarchy within the n submatrix entries of about two orders of magnitude. While not a generic feature of the ISS, this part of the parameter space can be motivated by anthropological arguments to avoid the overclosure of the Universe.

The right panel of Fig. 12 depicts the distribution of the generated baryon asymmetry in terms of the mixing angle $\theta_{\rm DM}$. We note that the small mixing angles required for reproducing the correct abundance of DM tend to generate a too small baryon asymmetry. This may be traced back to the tension between the preferred ranges for the mass splitting $\Delta m/m_{\rm PD}$ and the Yukawa couplings (see Fig. 7) and the relation (77). For small mixing angles with a strongly hierarchical structure of the submatrix n in Eq. (12), the eight-neutrino ISS(2,3) model effectively reduces to a toy model with only one RH and two sterile neutrinos, in particular there can be no cancellations in the matrix equations related to the sterile sector. In this case, Eq. (77) becomes an exact relation, implying that it is difficult to simultaneously obtain a suitable mass splitting, Yukawa coupling and heavy neutrino mass scale $m_{\rm PD}$. Both this analytical argument, as well as the numerical scan resulting in Fig. 12, suggest that while there may be a tuned region in parameter space which can generate both the correct DM abundance and baryon asymmetry, *generically* the ISS(2,3) cannot account for the baryon asymmetry of the Universe and its DM content simultaneously. We emphasize that

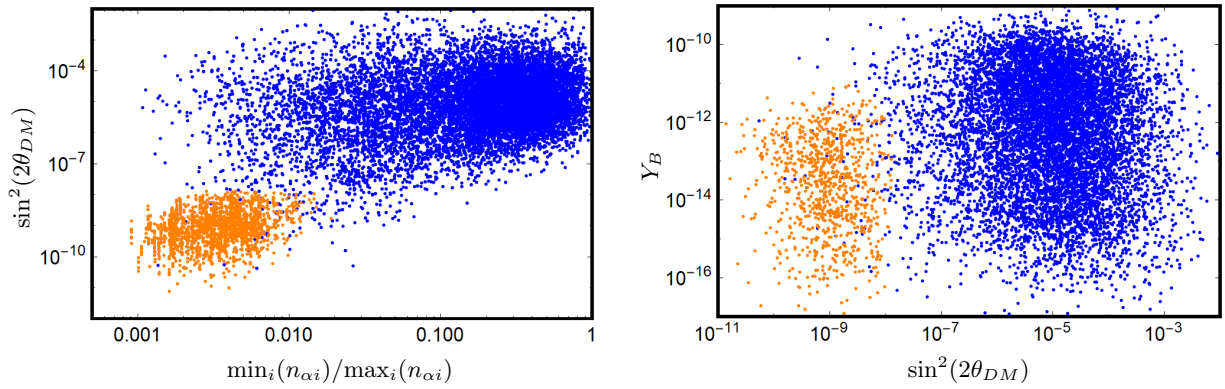

Figure 12: Mixing angle $\theta_{\rm DM}$ between the DM candidate and the active neutrinos. The blue points comply with all the constraints mentioned in Sec. 2.1 and provide a DM candidate in the suitable mass range, the yellow points in addition satisfy the DM related constraints of Ref. [23]. **Left panel**: Mixing angle versus hierarchy of the submatrix n in Eq. (12). **Right panel**: Generated baryon asymmetry versus mixing angle.

the ISS(2,3) generically overproduces DM when successful leptogenesis is imposed, hence without any additions to its cosmological history, the ISS(2,3) with a DM candidate in the keV range cannot be considered a successful setup for leptogenesis through neutrino oscillations.

Related work on the simultaneous explanation of the baryon asymmetry and DM of the Universe has been performed in the context of the νMSM [8,9], see e.g. [13] for a recent analysis. After producing the observed baryon asymmetry through neutrino oscillations, a second phase of leptogenesis is triggered at temperatures well below the EW phase transition. This generated lepton asymmetry is not transferred into the baryon sector, but instead strongly enhances the production of DM sterile neutrinos in the keV range. This production mechanism is dubbed resonant production or Shi-Fuller mechanism [10,11,121]. It allows for an efficient DM production for small enough mixing angles with the active neutrinos to comply with experimental limits. The Shi-Fuller mechanism requires a very efficient late time production of a lepton asymmetry and hence an extreme degeneracy for heavy RH neutrinos, corresponding in our notation to $\Delta m/m_{\rm PD} \sim 10^{-14}$ [13]. This mechanism is however not be at work in our framework, since these extremely small mass splittings cannot be generated within the ISS. Note that, given the systematically too large mixing-angles in the parameter region favored by leptogenesis, a Shi-Fuller production, if active, would further worsen the already severe issue of DM overproduction. For analogous reasons the freeze-in production mechanism suggested in [23, 122–124], sourced by the decay of heavy sterile states, is not a viable option in our setup.

A possible solution to the DM problem could be a late time entropy injection [125][13] diluting

[13]Notice that DM is produced through the DW mechanism at temperatures of the order of 100 MeV. Entropy injection should occur at lower temperatures and, consequently, much later than leptogenesis.

the DM abundance. This solution is however somewhat contrived since entropy injection would have analogous effect also on the baryon asymmetry. As shown in the right panel of Fig. 12, the baryon asymmetry of the upper most points exceed the observed value by about two orders of magnitude, however only few blue points can be brought into the cosmologically viable region by reducing $\sin^2(2\theta_{\rm DM})$ by two orders of magnitude. Alternatively, one could consider the case in which the DM is driven to thermal equilibrium, for example by additional gauge interactions [126, 127]. Thermal keV Dark Matter would also be overabundant; however the amount of entropy injection needed to set the current abundance is more moderate and still potentially compatible with the correct amount of baryon asymmetry (notice however that the extra interactions thermalizing the DM could also affect the leptogenesis process). A further option might be to suppress the DM - active neutrino oscillations in the early Universe by introducing a temperature-dependent neutrino mass term [128]. A full analysis of these possibilities is beyond the scope of this paper.

5 Conclusion

A central piece of this work is a new linearized formulation of the set of Boltzmann equations describing the generation of the baryon asymmetry of the Universe from CP-violating oscillations of nearly mass degenerate neutrino pairs with a GeV mass scale. The small mass splitting at the origin of the leptogenesis mechanism naturally emerges in extensions of the SM involving extra sterile/right-handed fermions, based on a small violation of lepton number. The refined system of Boltzmann equation allows to study leptogenesis beyond the weak washout regime, extending and completing the results presented in [17].

Our study was conducted in the framework of i) a minimal extension of the SM by two SM singlet fermions, the LSS-ISS, providing a natural explanation of their strong mass degeneracy based on two LNV parameters; ii) the Inverse Seesaw in its most minimal realization, the ISS (2,2), which features two pseudo-Dirac neutrino pairs beyond the SM states; iii) the ISS (2,3), which leads to a similar spectrum with an additional sterile state with mass around the keV, a possible DM candidate.

We present the parametrization and derivation of the new linearized kinetic equations based on Fermi-Dirac statistical distributions, including the impact of soft scatterings of gauge bosons in the thermal plasma and the presence of small leptonic chemical potentials. We also take into account the re-distribution of the asymmetry in the active sector through spectator processes. This new treatment enables a strong simplification of the system of differential equations, empowering a fast numerical solution, allowing in particular a full coverage of the parameter space in both the strong and weak washout regimes.

In the case of the LSS-ISS model, we find that the parameter space relevant for viable leptogenesis in the strong washout regime shows a preference for a relative mass splitting between the heavy

neutrinos of about $\Delta m/m_{\rm PD} \sim 10^{-4} - 10^{-3}$ and for Yukawa couplings $\lesssim 10^{-5}$. Contrary to the case of the weak washout regime which was the focus of [17], the viable model points in the strong washout regime lie within the expected sensitivity of planned future facilities like SHiP, FCC-ee and LBNF/DUNE. These experiments hence have the potential to discriminate between weak and strong washout regimes within this model.

In the case of the ISS, we focus on the possibility that the lighter pseudo-Dirac pair generates the lepton asymmetry, whereas the mass scale of the second pseudo-Dirac pair is taken to be much heavier, so that it effectively decouples during leptogenesis. In this setup we find similar results as in the LSS-ISS model, however the range of viable masses for the neutrino pair responsible of the generation of the lepton asymmetry is sensitively reduced. This is due to a tighter relations between the masses of the new neutrinos and their Yukawa couplings in the ISS framework. Larger masses correspond to larger Yukawa couplings, implying too strong washout effects.

In the final case of the ISS(2,3) model, viable leptogenesis is achieved in analogous regions of the parameter space as in the ISS(2,2). In addition, this model features the intriguing possibility of addressing at the same time the DM puzzle. This possibility appears however disfavored in this minimal realization of the ISS since the DM candidate is generically overproduced, implying an overclosure of the Universe unless the standard cosmological history is altered. Given the high dimensionality of the parameter space, we can however not exclude the existence of fine-tuned parameter combinations which might nevertheless achieve this task.

Acknowledgements

We thank M. Drewes and J. Lopez-Pavon for helpful discussions. A.A. acknowledges partial support from the European Union Horizon 2020 research and innovation programme under the Marie Skłodowska-Curie: RISE InvisiblesPlus (grant agreement n° 690575) and the ITN Elusives (grant agreement n° 674896). V.D. acknowledges the financial support of the UnivEarthS Labex program at Sorbonne Paris Cité (ANR-10-LABX-0023 and ANR-11-IDEX-0005-02), the Paris Centre for Cosmological Physics and the L'Oréal - Unesco program 'For Women in Science'. M.L. acknowledges support by the Fonds de la Recherche Scientifique - FNRS under Grant n° IISN 4.4512.10.

A Some useful formulas for simplifying the kinetic equations

This Appendix collects technical details and useful formulas supporting the derivations in Section 3.

A.1 Decay rates

The generic expression for the production process $a(E_1) + b(E_2) \to c(E_3) + N(p_N)$ involving one vertex associated with the Yukawa coupling F is given by:

$$\Gamma_N^d = \frac{1}{2k_N} F^\dagger \left(\int \left(\prod_{f=1}^{3} \frac{d^3 p_f}{(2\pi)^3} \right) (2\pi)^4 \delta(p_1 + p_2 - p_3 - p_N) |M|^2 f_a(E_1) f_b(E_2)(1 \pm f_c(E_3)) \right) F \ , \tag{81}$$

where $f_{f=a,b,c}$ are Fermi-Dirac (f_F) or Bose-Einstein (f_B) distributions. The destruction rate is given by:

$$\Gamma_N^p = \frac{1}{2k_N} F^\dagger \left(\int \left(\prod_{f}^{3} \frac{d^3 p_f}{(2\pi)^3} \right) (2\pi)^4 \delta(p_1 + p_2 - p_3 - p_N) |M|^2 (1 \pm f_a(E_1))(1 \pm f_b(E_2)) f_c(E_3) \right) F \ . \tag{82}$$

By using the following properties

$$\begin{aligned} f_B(E_1) f_B(E_2) &= f_B(E_1 + E_2)(1 + f_B(E_1) + f_B(E_2)) \, , \\ f_B(-E_1) &= -(1 + f_B(E_1)) \, , \\ f_F(E_1) &= -f_B(E_1 + i\pi T) \, , \end{aligned} \tag{83}$$

the products of Fermi-Dirac and Bose-Einstein distributions in Eqs. (81-82) can be rewritten:

$$f_a(E_1) f_b(E_2)(1 \pm f_c(E_3)) = f_F(x_N, \pm\mu) \hat{f} \widetilde{f} \ , \tag{84}$$

$$(1 \pm f_a(E_1))(1 \pm f_b(E_2)) f_c(E_3) = (1 - f_F(x_N, \pm\mu)) \hat{f} \widetilde{f} \ . \tag{85}$$

Notice that $\hat{f}$ and $\widetilde{f}$ are also functions of the chemical potential. The functions Σ and Ψ defined in the main text represent the coefficients of the expansion of Eq. (84) with respect to the chemical potential μ. By using the expression of the amplitudes given in [28] and expanding Eq. (84), we obtain:

$$\begin{aligned} \Sigma(x_N) &= \left(6h_t^2 F_s^{q\,(0)}(x_N) + (3g^2 + g'^2) \left(F_s^{V\,(0)}(x_N) + F_{t_1}^{V\,(0)}(x_N) + F_{t_2}^{V\,(0)}(x_N) \right) \right) \ , \\ \Psi(x_N) &= (3g^2 + g'^2) \left[(\delta F_{t_1,a}^V - \delta F_{t_1,b}^V) + (\delta F_{t_2,a}^V - \delta F_{t_2,b}^V) - (\delta F_{s,a}^V - \delta F_{s,b}^V) \right] - 6h_t^2 \delta F_s^q(x_N) \ , \end{aligned} \tag{86}$$

where:

$$\begin{aligned} F_s^{q\,(0)}(x_N) &= \int_{x_N}^{\infty} d\chi^+ \int_0^{x_N} d\chi^- \left(f_B^0(\chi^0) + f_F^0(\chi^0 - x_N) \right) \\ &\quad \left(\chi + 2 \left(\log(1 - \exp(-\chi^+)) - \log(1 + \exp(\chi^-)) \right) \right) \ , \end{aligned} \tag{87}$$

$$
\begin{aligned}
F_s^{V\,(0)}(x_N) &= \int_{x_N}^{\infty} d\chi^+ \int_0^{x_N} d\chi^- \left(f_B^0(\chi^0 - x_N) + f_F^0(\chi^0)\right) \\
&\left\{\frac{\chi}{2} - \frac{1}{\chi}\left[(x_N - \chi^+)\left(\log(1-\exp(-\chi^+)) - \log(1+\exp(-\chi^-))\right)\right.\right. \\
&\left.+(x_N - \chi^-)\left(\log(1-\exp(-\chi^-)) - \log(1+\exp(-\chi^+))\right)\right] \\
&-\frac{1}{\chi^2}(\chi^0 - 2x_N)\left[Li_2(\exp(-\chi^+)) - Li_2(\exp(-\chi^-)) - \right. \\
&\left.\left. Li_2(-\exp(-\chi^+)) + Li_2(-\exp(-\chi^+))\right]\right\} , \qquad (88) \\
F_{t_1}^{V\,(0)}(x_N) &= \int_0^{x_N} d\chi^+ \int_{-\infty}^{0} d\chi^- \left(1 + f_B^0(x_N - \chi^0) - f_F^0(\chi^0)\right) \\
&\left\{\frac{1}{\chi}(x_N - \chi^-)\left[\log(1+\exp(-\chi^+)) - \log(1-\exp(-\chi^-))\right]\right. \\
&\left.\frac{1}{\chi^2}(2x_N - \chi^0)\left[-Li_2(\exp(-\chi^+)) - Li_2(\exp(-\chi^-))\right]\right\} , \qquad (89) \\
F_{t_2}^{V\,(0)}(x_N) &= \int_0^{x_N} d\chi^+ \int_{-\infty}^{0} d\chi^- \left(1 + f_B^0(\chi^0) - f_F^0(x_N - \chi^0)\right) \\
&\left\{\frac{1}{\chi}(x_N - \chi^+)\left[-\log(1+\exp(-\chi^+)) + \log(1-\exp(\chi^-))\right]\right. \\
&\left.\frac{1}{\chi^2}(2x_N - \chi^0)\left[Li_2(\exp(-\chi^+)) - Li_2(-\exp(-\chi^-))\right]\right\} , \qquad (90)
\end{aligned}
$$

where $\chi^0 = \chi^+ + \chi^-$ and $\chi = \chi^+ - \chi^-$. Furthermore,

$$
\begin{aligned}
\delta F_{s,a}^V &= \int_{x_N}^{\infty} d\chi^+ \int_0^{x_N} d\chi^- f_F'(\chi^0) \left\{\frac{\chi}{2} - \frac{1}{\chi}\left[(x_N - \chi^+)\left(\log(1-\exp(-\chi^+)) - \log(1+\exp(-\chi^-))\right)\right.\right. \\
&\left.+(x_N - \chi^-)\left(\log(1-\exp(-\chi^-)) - \log(1+\exp(-\chi^+))\right)\right] \\
&-\frac{1}{\chi^2}(\chi^0 - 2x_N)\left[Li_2(\exp(-\chi^+)) - Li_2(\exp(-\chi^-))\right. \\
&\left.\left. -Li_2(-\exp(-\chi^+)) + Li_2(-\exp(-\chi^+))\right]\right\} , \qquad (91) \\
\delta F_{s,b}^V &= \int_{x_N}^{\infty} d\chi^+ \int_0^{x_N} d\chi^- \left(f_F^0(\chi^0) + f_B^0(\chi^0 - x_N)\right) \\
&\left\{-\frac{1}{\chi} f_B^0(\chi^+) f_B^0(\chi^-)\left[(x_N - \chi^+)\exp(\chi^-) + (x_N - \chi^-)\exp(\chi^+) + \exp(\chi)(\chi^0 - 2x_N)\right]\right. \\
&\left.-\frac{1}{\chi^2}(\chi^0 - 2x_N)\log\left[\frac{-1+\exp(\chi^-)}{-1+\exp(\chi^+)}\right]\right\} , \qquad (92) \\
\delta F_{t_1,a}^V &= \int_0^{x_N} d\chi^+ \int_{-\infty}^{0} d\chi^- f_F'(\chi^0) \\
&\left\{\frac{1}{\chi}(x_N - \chi^-)\left[\log(1+\exp(-\chi^+)) - \log(1-\exp(-\chi^-))\right]\right. \\
&\left.\frac{1}{\chi^2}(2x_N - \chi^0)\left[-Li_2(\exp(-\chi^+)) - Li_2(\exp(-\chi^-))\right]\right\} , \qquad (93)
\end{aligned}
$$

$$
\begin{aligned}
\delta F^V_{t_1,b} &= \int_0^{x_N} d\chi^+ \int_{-\infty}^0 d\chi^- \left(1 + f^0_B(x_N - \chi^0) - f^0_F(\chi^0)\right) \\
&\left\{\frac{1}{\chi}\left[f^0_F(\chi^-)(\chi^- - x_N) - \frac{\chi^+}{\chi}(\chi^0 - 2x_N)\right]\right. \\
&\left.\frac{1}{\chi^2}(\chi^0 - 2x_N)\log(1+\exp(\chi^+))\right\} \ , \qquad (94) \\
\delta F^V_{t_2,a} &= \int_0^{x_N} d\chi^+ \int_{-\infty}^0 d\chi^- f'_B(\chi^0) \\
&\left\{\frac{1}{\chi}(x_N - \chi^+)\left[-\log(1+\exp(-\chi^+)) + \log(1-\exp(\chi^-))\right]\right. \\
&\left.\frac{1}{\chi^2}(2x_N - \chi^0)\left[Li_2(\exp(-\chi^+)) - Li_2(-\exp(-\chi^-))\right]\right\} \ , \qquad (95) \\
\delta F^V_{t_2,b} &= \int_0^{x_N} d\chi^+ \int_{-\infty}^0 d\chi^- \left(1 + f^0_B(\chi^0) - f^0_F(x_N - \chi^0)\right) \\
&\left\{\frac{1}{\chi} f^0_F(\chi^-)\exp(-\chi^-)(\chi^- - x_N) + \frac{1}{\chi^2}(\chi^0 - 2x_N)\log(1+\exp(-\chi^-))\right\} \ . \qquad (96)
\end{aligned}
$$

To rephrase the differential equations in terms of thermally averaged decay rates and to compare with earlier works based on the Maxwell-Boltzmann distribution $f_{\rm B}$, some useful relations are

$$
\begin{aligned}
&\int \frac{d^3k}{(2\pi)^3} f^0_F(k/T) = \frac{3T^3\zeta(3)}{4\pi^2} \ , \qquad \int \frac{d^3k}{(2\pi)^3} f'_F(k/T) = -\frac{T^3}{12} \ , \qquad \int \frac{d^3k}{(2\pi)^3}\frac{f^0_F(k/T)}{k} = \frac{T^2}{24} \ , \\
&\int \frac{d^3k}{(2\pi)^3} f^0_{\rm B}(k/T) = \frac{T^3}{\pi^2} \ , \qquad \int \frac{d^3k}{(2\pi)^3} f'_{\rm B}(k/T) = -\frac{T^3}{\pi^2} \ . \qquad (97)
\end{aligned}
$$

A.2 Weak washout limit

In this subsection we will briefly present the derivation of the expression in Eq. (35) for the baryon asymmetry in the weak washout regime. The procedure substantially coincides with the one already discussed in [17]. Differently to this reference we will adopt the Fermi-Dirac distributions for neutrinos and active leptons and include in the interaction rates the processes relying on gauge interactions.

The weak washout limit solution is obtained through a perturbative expansion of the system of Eqs. (27-28). As a first step, the equation for the neutrino density is solved at the lowest order, i.e. neglecting the chemical potential and approximating $R_N - I \approx I$:

$$
\frac{dR_N}{dt} = -i\left[\langle H\rangle, R_N\right] + \langle\Gamma^0\rangle F^\dagger F \ . \qquad (98)
$$

Eliminating the oscillation term through the transformation $R_N = E(t)\widetilde{R}_N E^\dagger(t)$, the equation is straightforwardly solved for:

$$
\widetilde{R}_N = \int_0^t dt_1 \langle\Gamma^0\rangle(t_1) E(t_1) F^\dagger F E(t_1) \ . \qquad (99)
$$

This solution is substituted in the leading order equation for the chemical potentials which read, taking again the lowest order contributions:

$$\frac{d\mu_{\Delta_\alpha}}{dt} = -\frac{9\zeta(3)}{2N_D\,\pi^2}\langle\Gamma^0\rangle\left(FR_NF^\dagger - F^*R_{\bar{N}}F^T\right) \ . \tag{100}$$

This can be directly integrated:

$$\begin{aligned}\mu_{\Delta_\alpha} &= -\frac{9\zeta(3)}{2N_D\pi^2}\int_0^t dt_1\langle\Gamma^0\rangle(t_1)\int_0^{t_1} dt_2\langle\Gamma^0\rangle(t_2)\Big[FE(t_1)E(t_2)^\dagger F^\dagger FE(t_2)E(t_1)^\dagger F^\dagger \\ &\quad -F^*E(t_1)E(t_2)^\dagger F^T F^*E(t_2)E(t_1)^\dagger F^T\Big]_{\alpha\alpha} \\ &= -\frac{9\zeta(3)}{2N_D\pi^2}\delta_\alpha\int_0^t dt_1\langle\Gamma^0\rangle\int_0^{t_1}\langle\Gamma^0\rangle(t_2)\sin\left(\int_{t_2}^{t_1} dt_3E_2(t_3)-E_3(t_3)\right) \ ,\end{aligned} \tag{101}$$

where

$$\int_{t_2}^{t_3} dt_3E_2(t_3)-E_3(t_3) = z(T_1)-z(T_2) \ , \tag{102}$$

with

$$z(T) = \frac{T_L^3}{T^3}, \quad T_L = \left(\frac{1}{12}\frac{\pi^2}{9\zeta(3)}M_0\Delta M^2\right)^{1/3} \ . \tag{103}$$

Using this last result, we find

$$\mu_{\Delta\alpha} = -\frac{9}{2}\frac{\zeta(3)}{N_D\pi^2}\delta_\alpha\left(\frac{M_0}{T_L}\right)^2\left(\frac{\pi}{1152\zeta(3)}\right)^2\widetilde{J}_{32}\left(\frac{T_L}{T}\right) \ , \tag{104}$$

where

$$\begin{aligned}\widetilde{J}_{32}(x) &= \int_0^x dx_1c_0(x_1)\int_0^{x_1} dx_2c_0(x_2)\sin\left(x_1^3-x_2^3\right) \ , \\ c_0(x) &= c_Q^{(0)}h_t^2 + c_{\rm LPM}^{(0)} + \left(3g^2\left(\pi\frac{T_L}{x}\right)+g'^2\left(\pi\frac{T_L}{x}\right)\right)\times \\ &\qquad \left(c_V^{(0)}+\log\left(\frac{1}{3g^2\left(\pi\frac{T_L}{x}\right)+g'^2\left(\pi\frac{T_L}{x}\right)}\right)\right) \ .\end{aligned} \tag{105}$$

The last step is the solution for the asymmetry ΔR in the sterile neutrinos:

$$\frac{d\Delta R_{II}}{dt} = 2\langle\Gamma^{(1)}\rangle\left(F^\dagger A_{\alpha\beta}\mu_{\Delta\beta}F\right)_{II} \ , \tag{106}$$

which again can be directly integrated,

$$(\Delta R)_{II} = -9\frac{\zeta(3)}{N_D\pi^2}\left(\frac{\pi}{2304\zeta(3)}\right)^3\left(\frac{M_0}{T_L}\right)^3\left(F^\dagger A_{\alpha\beta}\delta_\beta F\right)_{II}\int_0^x dx_1c_1(x_1)\widetilde{J}_{32}(x) \ , \tag{107}$$

with

$$\begin{aligned}c_1(x) &= c_Q^{(1)}h_t^2 + c_{\rm LPM}^{(1)} + \left(3g^2\left(\pi\frac{T_L}{x}\right)+g'^2\left(\pi\frac{T_L}{x}\right)\right) \\ &\qquad \times\left(c_V^{(1)}+\log\left(\frac{1}{3g^2\left(\pi\frac{T_L}{x}\right)+g'^2\left(\pi\frac{T_L}{x}\right)}\right)\right) \ .\end{aligned} \tag{108}$$

Assuming negligible variation with the temperature of the functions c_0 and c_1, and defining

$$\frac{\left(c_0^2\, c_1\right)^{1/3}}{2304} = \frac{\sin\phi}{8}\ , \tag{109}$$

the result simplifies to:

$$(\Delta R)_{II}\,(T) = -\frac{9\pi^{7/6}}{512\,\zeta(3)^{4/3}\,\Gamma(5/6)}\frac{M_0}{T}\frac{M_0^{4/3}}{\Delta m^{4/3}}\sin^3\phi\left(F^\dagger A_{\alpha\beta}\delta_\beta F\right)_{II}\ , \tag{110}$$

so that the baryon abundance is given by:

$$Y_B = \frac{n_B}{s} = \frac{28}{79}Y_{N_0}\sum_I (\Delta R)_{II}\,(T_{\rm EW})\ , \tag{111}$$

with $Y_{N_0} = 0.022$ [17].

A.3 Diagonalization of the equation for the sterile sector

In this subsection, we derive the expression for the unitary matrix V_α, which describes a basis in which the equation (37) for the sterile sector is greatly simplified. We first perform a change of basis to absorb the oscillations induced by the vacuum Hamiltonian H_N^0:

$$R_N^{(0)} \mapsto \widetilde{R}_N^{(0)} = E^\dagger(x)R_N^{(0)}E(x)\,, \tag{112}$$

with

$$E(t) = \exp\left(-i\int_{t_i}^{t}\langle H_N^0\rangle(t')dt'\right)\ , \tag{113}$$

where the vacuum Hamiltonian of the sterile neutrinos is given by $(H_N^0)_{ij} = \sqrt{k_N^2 + M_i^2}\delta_{ij}$. Clearly this removes the vacuum commutator containing the vacuum Hamiltonian from Eq. (27):

$$\begin{aligned}\frac{dR_N}{dt} &= \frac{d}{dt}\left(E\widetilde{R}_N E^\dagger\right) && (114)\\ &= -i\langle H_N^0\rangle E\widetilde{R}_N E^\dagger + E\left(\frac{d}{dt}\widetilde{R}_N\right)E^\dagger + iE\widetilde{R}_N E^\dagger\langle H_N^0\rangle^\dagger && (115)\\ &= E\left(\frac{d}{dt}\widetilde{R}_N\right)E^\dagger - i\left[\langle H_N^0\rangle, R_N\right]\ , && (116)\end{aligned}$$

where we have exploited $[\langle H_N^0\rangle, E] = 0$. In the ultra-relativistic limit, H_N^0 is given by

$$H_N^0 \to \frac{1}{2k_N}{\rm diag}(0, \Delta M^2)\,, \tag{117}$$

where we have omitted a contribution proportional to the unity matrix as this drops out in the commutator. After performing the thermal average,

$$\langle H_0\rangle = \frac{x\pi^2}{36\zeta(3)T_{\rm EW}}{\rm diag}(0, \Delta M^2)\,, \tag{118}$$

we find

$$E(x) = \mathrm{diag}\left(1, \exp(-ir^3x^3)\right) \ , \quad r = T_L/T_{\mathrm{EW}} \ , \tag{119}$$

with

$$T_L^3 = \frac{\pi^2}{108\zeta(3)} M_0 \Delta M^2 \ . \tag{120}$$

All remaining operators on the right-hand side of Eq. (37) are now of the structure $E^\dagger(x)F^\dagger FE(x)$. We can thus perform a second change of basis by the unitary matrix $V(x)$ which diagonalizes all these remaining operators. After removing the remaining ambiguity in the choice of $V(x)$ by requiring the second row to be real and positive, $V(x)$ can be calculated explicitly. It is of the form

$$V(x,\alpha) = \begin{pmatrix} e^{i(\alpha - x^3r^3)} f_{11} & e^{i(\alpha - x^3r^3)} f_{12} \\ f_{21} & f_{22} \end{pmatrix} \ , \tag{121}$$

where f_{ij} are time-independent combinations of the absolute values of the matrix elements of $F^\dagger F$ and α denoting the phase of $(F^\dagger F)_{12}$. We see that in the total basis transformation by the matrix $E{\cdot}V$, the time (or equivalently temperature) dependence reduces to a global phase and hence cancels out in the unitary matrix transformation. We may thus replace $E(x)V(x,\alpha) \mapsto V_\alpha = V(x=0,\alpha)$.

Finally, exploiting

$$V^\dagger \frac{df}{dx} V = \frac{d}{dx}\left(V^\dagger f V\right) + \left[V^\dagger \frac{dV}{dx}, V^\dagger f V\right] \ , \tag{122}$$

which holds for any function $f(x)$ and unitary matrix $V(x)$, we arrive at Eq. (43) quoted in the main text. As mentioned in the main text, this introduces the matrix D, which is defined by

$$V^\dagger \dot{V} = x^2 D \ . \tag{123}$$

B The parameter space for DM in the ISS(2,3)

In Section 4.2.3, we observed that a small mixing angle between the active sector and the DM candidate (required to avoid overproducing DM in the DW mechanism), can be achieved by allowing for a sizable hierarchy within the submatrix n of Eq. (12). In this Appendix we explain this result analytically by considering a minimal toy model with one active flavor, one right-handed neutrino and two sterile fermions:

$$\mathcal{M} = \begin{pmatrix} 0 & \frac{1}{2}Yv & 0 & 0 \\ \frac{1}{2}Yv & 0 & n_1\Lambda & n_2\Lambda \\ 0 & n_1\Lambda & \xi_1\Lambda & 0 \\ 0 & n_2\Lambda & 0 & \xi_2\Lambda \end{pmatrix} \ . \tag{124}$$

For simplicity we will take all parameters to be real in the following. To leading order in Y and $\xi_{1,2}$, this mass matrix is diagonalized as

$$\mathcal{U}^T \mathcal{M} \mathcal{U} = \mathrm{diag}(0, m_{\mathrm{DM}}, m_{\mathrm{PD}} - m_{\mathrm{DM}}, m_{\mathrm{PD}} + m_{\mathrm{DM}}) \ , \tag{125}$$

with $m_{PD} = \sqrt{n_1^2 + n_2^2}\,\Lambda$ and $m_{DM} = \frac{n_1^2\xi_2 + n_2^2\xi_1}{n_1^2+n_2^2}\Lambda$. In this basis, the DM-active mixing is determined by the entry $\mathcal{U}_{12}$, i.e. by the first component of the (correctly normalized) eigenvector corresponding to the second eigenvalue in Eq. (125):

$$\sin^2(2\theta_{\mathrm{DM}}) = 4\mathcal{U}_{12}^2 \simeq \frac{2n_1^2 n_2^2 (\xi_1 - \xi_2)^2}{(n_1^2 + n_2^2)(n_1^2\xi^2 + n_2^2\xi_1)^2} \frac{v^2 Y^2}{\Lambda^2} \ . \tag{126}$$

If $n_{1,2}$ are order one parameters, this yields $\sin^2(2\theta_{\mathrm{DM}}) = \mathcal{O}(v^2Y^2/\Lambda^2) = \mathcal{O}(10^{-10} - 10^{-4})$ for $Y = \mathcal{O}(10^{-7} - 10^{-4})$. If on the other hand $n_1 \gg n_2$ (or vice versa), the mixing angle (which depends on the product of both entries) is suppressed, whereas the mass eigenvalues (dependent on the sum of both entries) are governed by the larger entry.

References

[1] S. Davidson, E. Nardi, and Y. Nir, "Leptogenesis", *Phys. Rept.* **466** (2008) 105–177, `arXiv:0802.2962 [hep-ph]`.

[2] P. Minkowski, "$\mu \to e\gamma$ at a Rate of One Out of 10^9 Muon Decays?", *Phys. Lett.* **B67** (1977) 421–428.

[3] M. Gell-Mann, P. Ramond, and R. Slansky, "Complex Spinors and Unified Theories", *Conf. Proc.* **C790927** (1979) 315–321, `arXiv:1306.4669 [hep-th]`.

[4] T. Yanagida, "Horizontal symmetry and masses of neutrinos", *Conf. Proc.* **C7902131** (1979) 95–99.

[5] S. L. Glashow, "The Future of Elementary Particle Physics", *NATO Sci. Ser. B* **61** (1980) 687.

[6] R. N. Mohapatra and G. Senjanovic, "Neutrino Mass and Spontaneous Parity Violation", *Phys. Rev. Lett.* **44** (1980) 912.

[7] E. K. Akhmedov, V. A. Rubakov, and A. Yu. Smirnov, "Baryogenesis via neutrino oscillations", *Phys. Rev. Lett.* **81** (1998) 1359–1362, `arXiv:hep-ph/9803255 [hep-ph]`.

[8] T. Asaka, S. Blanchet, and M. Shaposhnikov, "The nuMSM, dark matter and neutrino masses", *Phys. Lett.* **B631** (2005) 151–156, `arXiv:hep-ph/0503065 [hep-ph]`.

[9] T. Asaka and M. Shaposhnikov, "The nuMSM, dark matter and baryon asymmetry of the universe", *Phys. Lett.* **B620** (2005) 17–26, `arXiv:hep-ph/0505013 [hep-ph]`.

[10] M. Shaposhnikov, "The nuMSM, leptonic asymmetries, and properties of singlet fermions", *JHEP* **08** (2008) 008, `arXiv:0804.4542 [hep-ph]`.

[11] M. Laine and M. Shaposhnikov, "Sterile neutrino dark matter as a consequence of nuMSM-induced lepton asymmetry", *JCAP* **0806** (2008) 031, `arXiv:0804.4543 [hep-ph]`.

[12] L. Canetti, M. Drewes, and M. Shaposhnikov, "Sterile Neutrinos as the Origin of Dark and Baryonic Matter", *Phys. Rev. Lett.* **110** (2013) no. 6, 061801, `arXiv:1204.3902 [hep-ph]`.

[13] L. Canetti, M. Drewes, T. Frossard, and M. Shaposhnikov, "Dark Matter, Baryogenesis and Neutrino Oscillations from Right Handed Neutrinos", *Phys. Rev.* **D87** (2013) 093006, `arXiv:1208.4607 [hep-ph]`.

[14] M. Drewes and B. Garbrecht, "Leptogenesis from a GeV Seesaw without Mass Degeneracy", *JHEP* **03** (2013) 096, `arXiv:1206.5537 [hep-ph]`.

[15] L. Canetti, M. Drewes, and B. Garbrecht, "Probing leptogenesis with GeV-scale sterile neutrinos at LHCb and Belle II", *Phys. Rev.* **D90** (2014) no. 12, 125005, `arXiv:1404.7114 [hep-ph]`.

[16] P. Hernández, M. Kekic, J. López-Pavón, J. Racker, and N. Rius, "Leptogenesis in GeV scale seesaw models", *JHEP* **10** (2015) 067, `arXiv:1508.03676 [hep-ph]`.

[17] A. Abada, G. Arcadi, V. Domcke, and M. Lucente, "Lepton number violation as a key to low-scale leptogenesis", *JCAP* **1511** (2015) no. 11, 041, `arXiv:1507.06215 [hep-ph]`.

[18] P. Hernández, M. Kekic, J. López-Pavón, J. Racker, and J. Salvado, "Testable Baryogenesis in Seesaw Models", *JHEP* **08** (2016) 157, `arXiv:1606.06719 [hep-ph]`.

[19] M. Shaposhnikov, "A Possible symmetry of the nuMSM", *Nucl. Phys.* **B763** (2007) 49–59, `arXiv:hep-ph/0605047 [hep-ph]`.

[20] D. Wyler and L. Wolfenstein, "Massless Neutrinos in Left-Right Symmetric Models", *Nucl. Phys.* **B218** (1983) 205–214.

[21] R. N. Mohapatra and J. W. F. Valle, "Neutrino Mass and Baryon Number Nonconservation in Superstring Models", *Phys. Rev.* **D34** (1986) 1642.

[22] A. Abada and M. Lucente, "Looking for the minimal inverse seesaw realisation", *Nucl. Phys.* **B885** (2014) 651–678, `arXiv:1401.1507 [hep-ph]`.

[23] A. Abada, G. Arcadi, and M. Lucente, "Dark Matter in the minimal Inverse Seesaw mechanism", *JCAP* **1410** (2014) 001, `arXiv:1406.6556 [hep-ph]`.

[24] V. De Romeri, E. Fernandez-Martinez, J. Gehrlein, P. A. N. Machado, and V. Niro, "Dark Matter and the elusive $\mathbf{Z}'$ in a dynamical Inverse Seesaw scenario", `arXiv:1707.08606 [hep-ph]`.

[25] S. M. Barr, "A Different seesaw formula for neutrino masses", *Phys. Rev. Lett.* **92** (2004) 101601, `arXiv:hep-ph/0309152 [hep-ph]`.

[26] M. Malinsky, J. C. Romao, and J. W. F. Valle, "Novel supersymmetric SO(10) seesaw mechanism", *Phys. Rev. Lett.* **95** (2005) 161801, `arXiv:hep-ph/0506296 [hep-ph]`.

[27] M. Drewes, B. Garbrecht, D. Gueter, and J. Klaric, "Leptogenesis from Oscillations of Heavy Neutrinos with Large Mixing Angles", *JHEP* **12** (2016) 150, `arXiv:1606.06690 [hep-ph]`.

[28] A. Anisimov, D. Besak, and D. Bodeker, "Thermal production of relativistic Majorana neutrinos: Strong enhancement by multiple soft scattering", *JCAP* **1103** (2011) 042, `arXiv:1012.3784 [hep-ph]`.

[29] D. Besak and D. Bodeker, "Thermal production of ultrarelativistic right-handed neutrinos: Complete leading-order results", *JCAP* **1203** (2012) 029, `arXiv:1202.1288 [hep-ph]`.

[30] J. Lopez-Pavon, S. Pascoli, and C.-f. Wong, "Can heavy neutrinos dominate neutrinoless double beta decay?", *Phys. Rev.* **D87** (2013) no. 9, 093007, `arXiv:1209.5342 [hep-ph]`.

[31] A. Abada, V. De Romeri, and A. M. Teixeira, "Effect of steriles states on lepton magnetic moments and neutrinoless double beta decay", *JHEP* **09** (2014) 074, `arXiv:1406.6978 [hep-ph]`.

[32] M. Drewes and B. Garbrecht, "Experimental and cosmological constraints on heavy neutrinos", `arXiv:1502.00477 [hep-ph]`.

[33] M. C. Gonzalez-Garcia, M. Maltoni, and T. Schwetz, "Global Analyses of Neutrino Oscillation Experiments", *Nucl. Phys.* **B908** (2016) 199–217, `arXiv:1512.06856 [hep-ph]`.

[34] I. Esteban, M. C. Gonzalez-Garcia, M. Maltoni, I. Martinez-Soler, and T. Schwetz, "Updated fit to three neutrino mixing: exploring the accelerator-reactor complementarity", *JHEP* **01** (2017) 087, `arXiv:1611.01514 [hep-ph]`.

[35] M. S. Chanowitz, M. A. Furman, and I. Hinchliffe, "Weak Interactions of Ultraheavy Fermions. 2.", *Nucl. Phys.* **B153** (1979) 402–430.

[36] L. Durand, J. M. Johnson, and J. L. Lopez, "Perturbative Unitarity Revisited: A New Upper Bound on the Higgs Boson Mass", *Phys. Rev. Lett.* **64** (1990) 1215.

[37] J. G. Korner, A. Pilaftsis, and K. Schilcher, "Leptonic flavor changing Z0 decays in SU(2) x U(1) theories with right-handed neutrinos", *Phys. Lett.* **B300** (1993) 381–386, `arXiv:hep-ph/9301290 [hep-ph]`.

[38] J. Bernabeu, J. G. Korner, A. Pilaftsis, and K. Schilcher, "Universality breaking effects in leptonic Z decays", *Phys. Rev. Lett.* **71** (1993) 2695–2698, `arXiv:hep-ph/9307295 [hep-ph]`.

[39] S. Fajfer and A. Ilakovac, "Lepton flavor violation in light hadron decays", *Phys. Rev.* **D57** (1998) 4219–4235.

[40] A. Ilakovac, "Lepton flavor violation in the standard model extended by heavy singlet Dirac neutrinos", *Phys. Rev.* **D62** (2000) 036010, `arXiv:hep-ph/9910213 [hep-ph]`.

[41] E. Akhmedov, A. Kartavtsev, M. Lindner, L. Michaels, and J. Smirnov, "Improving Electro-Weak Fits with TeV-scale Sterile Neutrinos", *JHEP* **05** (2013) 081, `arXiv:1302.1872 [hep-ph]`.

[42] L. Basso, O. Fischer, and J. J. van der Bij, "Precision tests of unitarity in leptonic mixing", *Europhys. Lett.* **105** (2014) no. 1, 11001, `arXiv:1310.2057 [hep-ph]`.

[43] E. Fernandez-Martinez, J. Hernandez-Garcia, J. Lopez-Pavon, and M. Lucente, "Loop level constraints on Seesaw neutrino mixing", *JHEP* **10** (2015) 130, `arXiv:1508.03051 [hep-ph]`.

[44] A. Abada, A. M. Teixeira, A. Vicente, and C. Weiland, "Sterile neutrinos in leptonic and semileptonic decays", *JHEP* **02** (2014) 091, `arXiv:1311.2830 [hep-ph]`.

[45] S. Antusch, J. P. Baumann, and E. Fernandez-Martinez, "Non-Standard Neutrino Interactions with Matter from Physics Beyond the Standard Model", *Nucl. Phys.* **B810** (2009) 369–388, `arXiv:0807.1003 [hep-ph]`.

[46] S. Antusch and O. Fischer, "Non-unitarity of the leptonic mixing matrix: Present bounds and future sensitivities", *JHEP* **10** (2014) 094, `arXiv:1407.6607 [hep-ph]`.

[47] M. Blennow, P. Coloma, E. Fernandez-Martinez, J. Hernandez-Garcia, and J. Lopez-Pavon, "Non-Unitarity, sterile neutrinos, and Non-Standard neutrino Interactions", `arXiv:1609.08637 [hep-ph]`.

[48] E. Ma and A. Pramudita, "Flavor Changing Effective Neutral Current Couplings in the Weinberg-Salam Model", *Phys. Rev.* **D22** (1980) 214.

[49] M. Gronau, C. N. Leung, and J. L. Rosner, "Extending Limits on Neutral Heavy Leptons", *Phys. Rev.* **D29** (1984) 2539.

[50] A. Ilakovac and A. Pilaftsis, "Flavor violating charged lepton decays in seesaw-type models", *Nucl. Phys.* **B437** (1995) 491, `arXiv:hep-ph/9403398 [hep-ph]`.

[51] F. Deppisch and J. W. F. Valle, "Enhanced lepton flavor violation in the supersymmetric inverse seesaw model", *Phys. Rev.* **D72** (2005) 036001, `arXiv:hep-ph/0406040 [hep-ph]`.

[52] F. Deppisch, T. S. Kosmas, and J. W. F. Valle, "Enhanced mu- - e- conversion in nuclei in the inverse seesaw model", *Nucl. Phys.* **B752** (2006) 80–92, `arXiv:hep-ph/0512360 [hep-ph]`.

[53] D. N. Dinh, A. Ibarra, E. Molinaro, and S. T. Petcov, "The $\mu - e$ Conversion in Nuclei, $\mu \to e\gamma, \mu \to 3e$ Decays and TeV Scale See-Saw Scenarios of Neutrino Mass Generation", *JHEP* **08** (2012) 125, `arXiv:1205.4671 [hep-ph]`. [Erratum: JHEP09,023(2013)].

[54] R. Alonso, M. Dhen, M. B. Gavela, and T. Hambye, "Muon conversion to electron in nuclei in type-I seesaw models", *JHEP* **01** (2013) 118, `arXiv:1209.2679 [hep-ph]`.

[55] A. Abada, M. E. Krauss, W. Porod, F. Staub, A. Vicente, and C. Weiland, "Lepton flavor violation in low-scale seesaw models: SUSY and non-SUSY contributions", *JHEP* **11** (2014) 048, `arXiv:1408.0138 [hep-ph]`.

[56] A. Abada, V. De Romeri, and A. M. Teixeira, "Impact of sterile neutrinos on nuclear-assisted cLFV processes", *JHEP* **02** (2016) 083, `arXiv:1510.06657 [hep-ph]`.

[57] E. Arganda, M. J. Herrero, X. Marcano, and C. Weiland, "Imprints of massive inverse seesaw model neutrinos in lepton flavor violating Higgs boson decays", *Phys. Rev.* **D91** (2015) no. 1, 015001, `arXiv:1405.4300 [hep-ph]`.

[58] F. F. Deppisch, P. S. Bhupal Dev, and A. Pilaftsis, "Neutrinos and Collider Physics", *New J. Phys.* **17** (2015) no. 7, 075019, `arXiv:1502.06541 [hep-ph]`.

[59] S. Banerjee, P. S. B. Dev, A. Ibarra, T. Mandal, and M. Mitra, "Prospects of Heavy Neutrino Searches at Future Lepton Colliders", *Phys. Rev.* **D92** (2015) 075002, `arXiv:1503.05491 [hep-ph]`.

[60] P. S. Bhupal Dev, R. Franceschini, and R. N. Mohapatra, "Bounds on TeV Seesaw Models from LHC Higgs Data", *Phys. Rev.* **D86** (2012) 093010, `arXiv:1207.2756 [hep-ph]`.

[61] C. G. Cely, A. Ibarra, E. Molinaro, and S. T. Petcov, "Higgs Decays in the Low Scale Type I See-Saw Model", *Phys. Lett.* **B718** (2013) 957–964, `arXiv:1208.3654 [hep-ph]`.

[62] P. Bandyopadhyay, E. J. Chun, H. Okada, and J.-C. Park, "Higgs Signatures in Inverse Seesaw Model at the LHC", *JHEP* **01** (2013) 079, `arXiv:1209.4803 [hep-ph]`.

[63] J. I. Illana and T. Riemann, "Charged lepton flavor violation from massive neutrinos in Z decays", *Phys. Rev.* **D63** (2001) 053004, `arXiv:hep-ph/0010193 [hep-ph]`.

[64] A. Abada, V. De Romeri, S. Monteil, J. Orloff, and A. M. Teixeira, "Indirect searches for sterile neutrinos at a high-luminosity Z-factory", *JHEP* **04** (2015) 051, `arXiv:1412.6322 [hep-ph]`.

[65] A. Abada, D. Bečirević, M. Lucente, and O. Sumensari, "Lepton flavor violating decays of vector quarkonia and of the Z boson", *Phys. Rev.* **D91** (2015) no. 11, 113013, `arXiv:1503.04159 [hep-ph]`.

[66] V. De Romeri, M. J. Herrero, X. Marcano, and F. Scarcella, "Lepton flavor violating Z decays: A promising window to low scale seesaw neutrinos", *Phys. Rev.* **D95** (2017) no. 7, 075028, `arXiv:1607.05257 [hep-ph]`.

[67] R. E. Shrock, "New Tests For, and Bounds On, Neutrino Masses and Lepton Mixing", *Phys. Lett.* **96B** (1980) 159–164.

[68] R. E. Shrock, "General Theory of Weak Leptonic and Semileptonic Decays. 1. Leptonic Pseudoscalar Meson Decays, with Associated Tests For, and Bounds on, Neutrino Masses and Lepton Mixing", *Phys. Rev.* **D24** (1981) 1232.

[69] A. Atre, T. Han, S. Pascoli, and B. Zhang, "The Search for Heavy Majorana Neutrinos", *JHEP* **05** (2009) 030, `arXiv:0901.3589 [hep-ph]`.

[70] A. Abada, D. Das, A. M. Teixeira, A. Vicente, and C. Weiland, "Tree-level lepton universality violation in the presence of sterile neutrinos: impact for R_K and R_π", *JHEP* **02** (2013) 048, `arXiv:1211.3052 [hep-ph]`.

[71] A. de Gouvea and S. Gopalakrishna, "Low-energy neutrino Majorana phases and charged-lepton electric dipole moments", *Phys. Rev.* **D72** (2005) 093008, `arXiv:hep-ph/0508148 [hep-ph]`.

[72] A. Abada and T. Toma, "Electric Dipole Moments of Charged Leptons with Sterile Fermions", *JHEP* **02** (2016) 174, `arXiv:1511.03265 [hep-ph]`.

[73] A. Abada and T. Toma, "Electron electric dipole moment in Inverse Seesaw models", *JHEP* **08** (2016) 079, arXiv:1605.07643 [hep-ph].

[74] A. Kusenko, "Sterile neutrinos: The Dark side of the light fermions", *Phys. Rept.* **481** (2009) 1–28, arXiv:0906.2968 [hep-ph].

[75] NA62 Collaboration, F. Hahn, F. Ambrosino, A. Ceccucci, H. Danielsson, N. Doble, F. Fantechi, A. Kluge, C. Lazzeroni, M. Lenti, G. Ruggiero, M. Sozzi, P. Valente, and R. Wanke, "NA62: Technical Design Document", NA62-10-07, CERN, Geneva, Dec, 2010. https://cds.cern.ch/record/1404985.

[76] SHiP, M. Anelli *et al.*, "A facility to Search for Hidden Particles (SHiP) at the CERN SPS", arXiv:1504.04956 [physics.ins-det].

[77] S. Alekhin *et al.*, "A facility to Search for Hidden Particles at the CERN SPS: the SHiP physics case", *Rept. Prog. Phys.* **79** (2016) no. 12, 124201, arXiv:1504.04855 [hep-ph].

[78] FCC-ee study Team, A. Blondel, E. Graverini, N. Serra, and M. Shaposhnikov, "Search for Heavy Right Handed Neutrinos at the FCC-ee", *Nucl. Part. Phys. Proc.* **273-275** (2016) 1883–1890, arXiv:1411.5230 [hep-ex].

[79] LBNE, C. Adams *et al.*, "The Long-Baseline Neutrino Experiment: Exploring Fundamental Symmetries of the Universe", arXiv:1307.7335 [hep-ex].

[80] F. F. Deppisch, M. Hirsch, and H. Pas, "Neutrinoless Double Beta Decay and Physics Beyond the Standard Model", *J. Phys.* **G39** (2012) 124007, arXiv:1208.0727 [hep-ph].

[81] M. Blennow, E. Fernandez-Martinez, J. Lopez-Pavon, and J. Menendez, "Neutrinoless double beta decay in seesaw models", *JHEP* **07** (2010) 096, arXiv:1005.3240 [hep-ph].

[82] EXO-200, J. B. Albert *et al.*, "Search for Majorana neutrinos with the first two years of EXO-200 data", *Nature* **510** (2014) 229–234, arXiv:1402.6956 [nucl-ex].

[83] KamLAND-Zen, A. Gando *et al.*, "Search for Majorana Neutrinos near the Inverted Mass Hierarchy Region with KamLAND-Zen", *Phys. Rev. Lett.* **117** (2016) no. 8, 082503, arXiv:1605.02889 [hep-ex]. [Addendum: Phys. Rev. Lett.117,no.10,109903(2016)].

[84] G. Sigl and G. Raffelt, "General kinetic description of relativistic mixed neutrinos", *Nucl. Phys.* **B406** (1993) 423–451.

[85] P. S. B. Dev and A. Pilaftsis, "Minimal Radiative Neutrino Mass Mechanism for Inverse Seesaw Models", *Phys. Rev.* **D86** (2012) 113001, arXiv:1209.4051 [hep-ph].

[86] S. Gariazzo, C. Giunti, M. Laveder, Y. F. Li, and E. M. Zavanin, "Light sterile neutrinos", *J. Phys.* **G43** (2016) 033001, arXiv:1507.08204 [hep-ph].

[87] A. A. Klypin, A. V. Kravtsov, O. Valenzuela, and F. Prada, "Where are the missing Galactic satellites?", *Astrophys. J.* **522** (1999) 82–92, arXiv:astro-ph/9901240 [astro-ph].

[88] B. Moore, S. Ghigna, F. Governato, G. Lake, T. R. Quinn, J. Stadel, and P. Tozzi, "Dark matter substructure within galactic halos", *Astrophys. J.* **524** (1999) L19–L22, arXiv:astro-ph/9907411 [astro-ph].

[89] L. E. Strigari, C. S. Frenk, and S. D. M. White, "Kinematics of Milky Way Satellites in a Lambda Cold Dark Matter Universe", *Mon. Not. Roy. Astron. Soc.* **408** (2010) 2364–2372, arXiv:1003.4268 [astro-ph.CO].

[90] M. Boylan-Kolchin, J. S. Bullock, and M. Kaplinghat, "Too big to fail? The puzzling darkness of massive Milky Way subhaloes", *Mon. Not. Roy. Astron. Soc.* **415** (2011) L40, arXiv:1103.0007 [astro-ph.CO].

[91] J. Baur, N. Palanque-Delabrouille, C. Yèche, C. Magneville, and M. Viel, "Lyman-alpha Forests cool Warm Dark Matter", *JCAP* **1608** (2016) no. 08, 012, arXiv:1512.01981 [astro-ph.CO].

[92] A. Merle and M. Totzauer, "keV Sterile Neutrino Dark Matter from Singlet Scalar Decays: Basic Concepts and Subtle Features", *JCAP* **1506** (2015) 011, arXiv:1502.01011 [hep-ph].

[93] J. König, A. Merle, and M. Totzauer, "keV Sterile Neutrino Dark Matter from Singlet Scalar Decays: The Most General Case", *JCAP* **1611** (2016) no. 11, 038, arXiv:1609.01289 [hep-ph].

[94] R. Murgia, A. Merle, M. Viel, M. Totzauer, and A. Schneider, ""Non-cold" dark matter at small scales: a general approach", arXiv:1704.07838 [astro-ph.CO].

[95] P. B. Pal and L. Wolfenstein, "Radiative Decays of Massive Neutrinos", *Phys. Rev.* **D25** (1982) 766.

[96] A. Boyarsky, A. Neronov, O. Ruchayskiy, and M. Shaposhnikov, "Constraints on sterile neutrino as a dark matter candidate from the diffuse x-ray background", *Mon. Not. Roy. Astron. Soc.* **370** (2006) 213–218, arXiv:astro-ph/0512509 [astro-ph].

[97] A. Boyarsky, D. Iakubovskyi, and O. Ruchayskiy, "Next decade of sterile neutrino studies", *Phys. Dark Univ.* **1** (2012) 136–154, arXiv:1306.4954 [astro-ph.CO].

[98] E. Bulbul, M. Markevitch, A. Foster, R. K. Smith, M. Loewenstein, and S. W. Randall, "Detection of An Unidentified Emission Line in the Stacked X-ray spectrum of Galaxy Clusters", *Astrophys. J.* **789** (2014) 13, `arXiv:1402.2301 [astro-ph.CO]`.

[99] A. Boyarsky, O. Ruchayskiy, D. Iakubovskyi, and J. Franse, "Unidentified Line in X-Ray Spectra of the Andromeda Galaxy and Perseus Galaxy Cluster", *Phys. Rev. Lett.* **113** (2014) 251301, `arXiv:1402.4119 [astro-ph.CO]`.

[100] L. Wolfenstein, "Neutrino Oscillations in Matter", *Phys. Rev.* **D17** (1978) 2369–2374.

[101] T. Asaka, S. Eijima, and H. Ishida, "Kinetic Equations for Baryogenesis via Sterile Neutrino Oscillation", *JCAP* **1202** (2012) 021, `arXiv:1112.5565 [hep-ph]`.

[102] R. Barbieri, P. Creminelli, A. Strumia, and N. Tetradis, "Baryogenesis through leptogenesis", *Nucl. Phys.* **B575** (2000) 61–77, `arXiv:hep-ph/9911315 [hep-ph]`.

[103] W. Buchmuller and M. Plumacher, "Spectator processes and baryogenesis", *Phys. Lett.* **B511** (2001) 74–76, `arXiv:hep-ph/0104189 [hep-ph]`.

[104] J. A. Harvey and M. S. Turner, "Cosmological baryon and lepton number in the presence of electroweak fermion number violation", *Phys. Rev.* **D42** (1990) 3344–3349.

[105] DUNE, R. Acciarri *et al.*, "Long-Baseline Neutrino Facility (LBNF) and Deep Underground Neutrino Experiment (DUNE)", `arXiv:1512.06148 [physics.ins-det]`.

[106] M. B. Gavela, T. Hambye, D. Hernandez, and P. Hernandez, "Minimal Flavour Seesaw Models", *JHEP* **09** (2009) 038, `arXiv:0906.1461 [hep-ph]`.

[107] F. L. Bezrukov, "nu MSM-predictions for neutrinoless double beta decay", *Phys. Rev.* **D72** (2005) 071303, `arXiv:hep-ph/0505247 [hep-ph]`.

[108] T. Asaka and S. Eijima, "Direct Search for Right-handed Neutrinos and Neutrinoless Double Beta Decay", *PTEP* **2013** (2013) no. 11, 113B02, `arXiv:1308.3550 [hep-ph]`.

[109] M. Drewes and S. Eijima, "Neutrinoless double β decay and low scale leptogenesis", *Phys. Lett.* **B763** (2016) 72–79, `arXiv:1606.06221 [hep-ph]`.

[110] T. Asaka, S. Eijima, and H. Ishida, "On neutrinoless double beta decay in the νMSM", *Phys. Lett.* **B762** (2016) 371–375, `arXiv:1606.06686 [hep-ph]`.

[111] Planck, P. A. R. Ade *et al.*, "Planck 2015 results. XIII. Cosmological parameters", *Astron. Astrophys.* **594** (2016) A13, `arXiv:1502.01589 [astro-ph.CO]`.

[112] A. Ceccucci, "Status and Plans of NA62." talk at the Invisibles17 Workshop, 2017.

[113] M. Drewes, B. Garbrecht, D. Gueter, and J. Klaric, "Testing the low scale seesaw and leptogenesis", arXiv:1609.09069 [hep-ph].

[114] J. A. Casas and A. Ibarra, "Oscillating neutrinos and muon —¿ e, gamma", *Nucl. Phys.* **B618** (2001) 171–204, arXiv:hep-ph/0103065 [hep-ph].

[115] S. Dodelson and L. M. Widrow, "Sterile-neutrinos as dark matter", *Phys. Rev. Lett.* **72** (1994) 17–20, arXiv:hep-ph/9303287 [hep-ph].

[116] T. Asaka, M. Laine, and M. Shaposhnikov, "Lightest sterile neutrino abundance within the nuMSM", *JHEP* **01** (2007) 091, arXiv:hep-ph/0612182 [hep-ph]. [Erratum: JHEP02,028(2015)].

[117] K. Abazajian, G. M. Fuller, and M. Patel, "Sterile neutrino hot, warm, and cold dark matter", *Phys. Rev.* **D64** (2001) 023501, arXiv:astro-ph/0101524 [astro-ph].

[118] S. Tremaine and J. E. Gunn, "Dynamical Role of Light Neutral Leptons in Cosmology", *Phys. Rev. Lett.* **42** (1979) 407–410.

[119] V. Domcke and A. Urbano, "Dwarf spheroidal galaxies as degenerate gas of free fermions", *JCAP* **1501** (2015) no. 01, 002, arXiv:1409.3167 [hep-ph].

[120] C. Di Paolo, F. Nesti, and F. L. Villante, "Phase space mass bound for fermionic dark matter from dwarf spheroidal galaxies", arXiv:1704.06644 [astro-ph.GA].

[121] X.-D. Shi and G. M. Fuller, "A New dark matter candidate: Nonthermal sterile neutrinos", *Phys. Rev. Lett.* **82** (1999) 2832–2835, arXiv:astro-ph/9810076 [astro-ph].

[122] T. Asaka, K. Ishiwata, and T. Moroi, "Right-handed sneutrino as cold dark matter", *Phys. Rev.* **D73** (2006) 051301, arXiv:hep-ph/0512118 [hep-ph].

[123] K. Petraki and A. Kusenko, "Dark-matter sterile neutrinos in models with a gauge singlet in the Higgs sector", *Phys. Rev.* **D77** (2008) 065014, arXiv:0711.4646 [hep-ph].

[124] L. J. Hall, K. Jedamzik, J. March-Russell, and S. M. West, "Freeze-In Production of FIMP Dark Matter", *JHEP* **03** (2010) 080, arXiv:0911.1120 [hep-ph].

[125] T. Asaka, M. Shaposhnikov, and A. Kusenko, "Opening a new window for warm dark matter", *Phys. Lett.* **B638** (2006) 401–406, arXiv:hep-ph/0602150 [hep-ph].

[126] F. Bezrukov, H. Hettmansperger, and M. Lindner, "keV sterile neutrino Dark Matter in gauge extensions of the Standard Model", *Phys. Rev.* **D81** (2010) 085032, arXiv:0912.4415 [hep-ph].

[127] M. Nemevsek, G. Senjanovic, and Y. Zhang, "Warm Dark Matter in Low Scale Left-Right Theory", *JCAP* **1207** (2012) 006, `arXiv:1205.0844 [hep-ph]`.

[128] F. Bezrukov, A. Chudaykin, and D. Gorbunov, "Hiding an elephant: heavy sterile neutrino with large mixing angle does not contradict cosmology", *JCAP* **1706** (2017) no. 06, 051, `arXiv:1705.02184 [hep-ph]`.